Postprint of: Dastjerdi, Sh, Malikan, M, Eremeyev, VA, Akgöz, B, Civalek, Ö., On the generalized model of shell structures with functional cross-sections, COMPOSITE STRUCTURES (2021), 114192, DOI: 10.1016/j.compstruct.2021.114192

On the generalized model of shell structures with functional cross-sections

Shahriar Dastjerdi [a], Mohammad Malikan [b], Victor A. Eremeyev [b,c,d *], Bekir Akgöz [a], Ömer Civalek [a,e]

[a] Division of Mechanics, Civil Engineering Department, Akdeniz University, Antalya, Turkey

[b] Department of Mechanics of Materials and Structures, Faculty of Civil and Environmental Engineering, Gdansk University of Technology, Gdansk, Poland

[c] Research and Education Center "Materials" Don State Technical University, Gagarina sq., 1, 344000 Rostov on Don, Russia

[d] DICAAR, Università degli Studi di Cagliari, Via Marengo, 2, 09123, Cagliari, Italy

[e] China Medical University, Taichung, Taiwan

* Corresponding author:

victor.eremeev@pg.edu.pl, eremeyev.victor@gmail.com

ABSTRACT

In the present study, a single general formulation has been presented for the analysis of various shell-shaped structures. The proposed model is comprehensive and a variety of theories can be used based on it. The cross-section of the shell structure can be arbitrarily analyzed with the presented equations. In other words, various types of shell structures, including cylindrical, conical, spherical, elliptical, hyperbolic, parabolic, and any non-geometric structure with

functional cross-section, can be modeled mechanically with only one partial differential equation system. The obtained equations have been solved by applying SAPM semi-analytical solution method. In order to present a comprehensive research, dynamic nonlinear analysis is considered. The variation of material properties through the thickness has been assumed as functionally graded and its effect on the strength of the shell structure with the functional cross-section has been investigated. The numerical results have been compared with available papers and also with FEM results for some structures that there is no paper available for validation. Different types of shell structures have been studied in terms of cross-sectional shape and properties. Finally, the effects of some important factors on the results such as boundary conditions, nonlinear analysis, dynamic analysis, and rotation of the structure around its central axis have been conducted thoroughly. This study and its original governing equations can be considered as a comprehensive reference for mechanical analysis of various shell structures with functional cross-sectional shape.

Keywords: Shell structures; Functional cross-section; Functionally graded material (FGM); SAPM methodology

1. Introduction

Mechanical analysis of shells has been a major part of more than three decades of research. Among them, cylindrical, spherical, and conical shells due to their application in various fields of engineering and advanced industries are among the topics of interest to researchers. In the classification of structures, spherical and cylindrical shells with very momentous applications in the field of engineering are of great importance. For example, cylindrical shells have a wide range of industrial applications, including centrifuges, turbines, dryers, tanks, electrical insulators, heat exchanger tubes, boilers, storage tanks, and so on. Spherical shells are also widely used in many structures, such as missiles, radar warheads, and

submarines. Conical shells, on the other hand, are broadly used because of the structural advantages they have in their geometry. For instance, they are employed in the oil, gas, and petrochemical industries. Therefore, the mathematical modeling of such structures is a significant issue.

Functionally graded materials (FGMs) are composite materials with a heterogeneous microstructure whose physical features vary softly along a given dimension based on the volume fraction. This special property is obtained by a uniform change in the volume ratio of their constituents. The microstructural phases of functionally graded materials have different functions from each other and cause a multi-structural state in functionally graded materials. With the intermittent and gradual change of the volume fraction of the ingredients of the functionally graded materials, these materials show the properties of a continuous substance. The most common type of these materials is ceramics and metals. As well as providing thermal protection and corrosion resistance on one surface, it also provides resistance to mechanical loads to the end of the other surface [1–5]. The idea of designing FGMs was first proposed by Japanese scientists as high-temperature resistant materials and was discussed at the first FGM conference [6–10]. FGMs, especially in shell form, are increasingly used in aerospace and other industries that require high strength and rigidity with low density. As the use of these materials in structures expanded, the need for further research on them became more apparent to researchers. Hence, the study of the mechanical behavior of FGM shells is a vital issue that must be addressed.

In the class of cylindrical shells, Shen [11–12] presented a thermo-mechanical post-stability study for FGM shells with a circular section regarding Donnell shell theory. The critical loads were determined by a singular perturbation technique. Amabili [13] examined nonlinear natural frequencies of cylindrical shells with circular cross-section while different shell theories

were taken into validation. Arciniega and Reddy [14] studied the nonlinear bending of shells composed of FGMs on the basis of the first-order theory of shear deformations. A shell element within the finite element method helped out to make the shell domain. Najafizadeh and Isvandzibaei [15] showed the importance of higher-order elasticity theories for vibrational modeling of shells composed of FGM in cylindrical coordinates. Darabi et al. [16] by imposing an axial periodic loading, inspected the dynamic stability of an FGM shell by making use of Donnell's theory. Shen [17] calculated the torsional critical load of shells produced by FGMs in a circular geometry. The temperature as an external factor was studied. A higher-order elasticity model was employed and numerical outcomes were attained by a singular perturbation method. Matsunaga [18] demonstrated the buckling and vibrational behavior of FGM shells with a circular cross-section. A higher-order elasticity model was utilized on the basis of two-dimensional assumptions in order to obtain governing equations. Kurylov and Amabili [19] investigated different boundary conditions for cylindrical shells put through nonlinear vibrations. Khalili et al. [20] on the basis of a novel modified three-dimensional elasticity model studied natural frequencies of a cylindrical shell. The shell had isotropic elastic behavior with homogeneity. The analytical solution established numerical results. Jin et al. [21] succeed to apply the Haar wavelet method on the model of cylindrical shells. Their shear deformable model involved FGMs properties. Mohammadi et al. [22] proposed a nano-sized shear deformable FGM shell with the cylindrical domain. The well-known nanoscale approach, which is a nonlocal strain gradient model supported the small-scale properties. Chen et al. [23] in the framework of FGM composition, implemented a cylindrical shell into a static buckling state, and probed the bifurcation behavior of the specimen. Sofiyev [24] studied buckling of cylindrical shells with visco-elastic material properties subjected to axial dynamic load. The elastic behavior for the cross-section was considered to be orthotropic. Hasrati et al. [25] presented a new solution technique based on the numerical process in order to investigate

natural and excitation frequencies of a cylindrical shell on the basis of geometrical nonlinearity. Khorsand et al. [26] enhanced the resistance of the cylindrical shells based upon a multi-directional FGM. Thermal gradient impressed the model and the functionality was undertaken with axial and radial directions. Ansari and Torabi [27] presented a semi-analytical solution for considering the post-stability of an FGM cylindrical shell when the graphene platelet played the role of a reinforcer. Malikan et al. [28] computed the capacity of torsional stability of a nano-sized shell containing magnetic properties in three dimensions by employing first-order shear deformation shell theory (FSDST). Karami and Janghorban [29] analyzed a supported nanoscale shell with simple boundaries in terms of FGMs property based on a quasi-three-dimensional shell model. Mohamadi et al. [30] conducted a nonlinear frequency analysis on axially moving the shells with cylindrical solid and circular cross-section inserted into simple boundary conditions. The shell motion equations were achieved on the basis of axial moving. For more considerations, one can find other interesting published works performed on cylindrical shells with a circular cross-section in [31–45].

In the category of spherical shells, Voyiadjis and Woelke [46] presented a modified elasticity theory to study the mechanics of thick spherical shells. Bich and Tung [47] considered the nonlinear behavior of an FGM spherical shell in the thermal environment subjected to an outer static pressure acted uniformly. Bich et al. [48] based on a nonlinear investigation, derived the classical model for FGM spherical shells by incorporating Donnell assumptions. Their study also consisted of thermal environment influences. Zaera et al. [49] investigated natural frequencies and vibration modes of a closed spherical shell in a nano-size based on the stress nonlocality model. Civalek [50] explored the geometrically nonlinear behavior of a spherical shell in static and dynamic conditions. The shell was held by a polymeric medium inclusive of shear and transverse stiffness. Fantuzzi et al. [51] expanded cylindrical as well as spherical shell panels into two- and three-dimensional analyses in the thin and thick cases. The shells were

deemed to be made by FGMs. The solution procedure was feasible with the aid of the finite element method and simply-supported ends conditions. Ghavanloo et al. [52] derived a shell model for fullerene molecules in order to compute the natural frequencies and vibration modes of the problem. Shinde and Sayyad [53] investigated a spherical shell assuming orthotropic elasticity and a fifth-order shear deformable shell model was assessed. Dastjerdi et al. [54] carried out a quasi-model for the human eye based on the viscoelastic spherical shell structures in the context of the first-order shell deformable model. There can be read some other articles in the case of shells with spherical geometry [55–56].

On studies of conical shells, Malekzadeh and Heydarpour [57] reviewed vibration modes and natural frequencies of an FGM shell with truncated conic geometry under rotation. The FSDST gave them constitutive equations and the differential quadrature method (DQM) came to their aid to solve the problem. Kamarian et al. [58] reinforced a conical shell with the help of carbon nanotubes and calculated vibration modes of the composite shell based on the FSDST deformable sample. Dai et al. [59] analyzed free vibration of a conical shell while it rotated around its vertical axis by taking into consideration the influences of Coriolis and centrifugal forces. Ansari et al. [60] estimated an FGM conical shell on the basis of graphene platelet as a reinforcer in a post-stability condition. Sofiyev [61] studied a composite truncated conical shell in static stability and vibrational conditions. The carbon nanotubes were embedded into the shell as a reinforcer and the mathematical model of the problem was performed regarding FSDST. Fu et al. [62] evaluated porosity in an FGM conical shell exposed to the thermo-dynamic environment. The first-order shear deformation shell approach and generalized differential quadrature technique created the mathematical process. Further interesting papers done for mechanics of conical shells can be seen in [63–70].

In the theme of special shell structures, Jiang and Redekop [71] studied the mechanical response of toroidal shells. The linear elastic behavior was supposed to be orthotropic. The shell was placed in both static and dynamic conditions and the mathematical model was solved with regard to the differential quadrature technique. The shell thickness was also presumed to be variable. Wang and Redekop [72] discussed natural frequencies of a shell with a toroidal section within moderately thick and thick hypotheses by FSDST and DQM. Shariyat and Asgari [73] analyzed nonlinear stability due to temperature for a bidirectional FGM shell with variable thickness and a circular section. Tornabene et al. [74] using the generalized differential quadrature method studied natural frequencies of elliptic and oval cylindrical shells. The shells were supposed to be composite material and the clamped-free end conditions were also surveyed. Bich and Ninh [75] studied a toroidal shell part made of FGMs counting classical shell theory in a post-stability status in regard to the environmental effects such as temperature variations. Their model was also reinforced by means of a polymer foundation. Torabi and Ansari [76] explored for frequency behavior of an FGM revolving shell based on an isoparametric super element within the framework of the three-dimensional finite element method. Dastjerdi et al. [77] developed shell studies by formulating a mathematical model of a torus-shaped shell on the base of FSDST. The materials properties were applied as FGMs and the system was also affected by hygro-thermal impacts of the environment. The numerical results were obtained by means of an innovative semi-analytical technique. Vuong and Duc [78] based on a nonlinear formulation, measured natural frequencies of a toroidal shell made of FGMs considering moderately thickness for the shell. Reddy's third order-shear deformation shell theory was utilized to create the mathematical model. Runge–Kutta method granted numerical results.

In the field of open-shell structures, Altenbach and Eremeyev [79] developed studies of open-shell structures into the nanoscale including surface effects. Tornabene [80] researched

the FGM doubly-curved shells with arbitrarily oriented rotation under critical speed. Different higher-order elasticity theories were examined to model the problem.

In the area of combined shells, Caresta and Kessissoglou [81] calculated natural frequencies of a shell constituted with cylindrical and conical geometries with respect to classical shell theories.

Mathematical analysis and modeling of shells has many problems and complexities. In addition, the number and methods presented add to these difficulties, and it is natural that the problems of shell analysis will be different due to their curvature in each shell. So far, most of the research done on shells has been limited to mathematical modeling of each shell separately. But in this paper, a mathematical model is presented by which all cylindrical, conical, revolved, and spherical shells with circular and elliptical sections, and curved cones can be mechanically simulated. In fact, with the mathematical model presented in this study, there is no need to model each shell separately with different models. In mechanical analysis, according to the physical characteristics of the problem and the loading, we use a nonlinear model when large deformations are considered. Therefore, in this paper, based on the first-order shear deformation shell theory, the mathematical model was investigated by considering the effect of nonlinear terms on the geometry of the shell. Environmental effects are one of the vital factors in the performance of industrial components made of different shells. These effects can be the result of fluid movement in a cylindrical or conical shell or a wet working environment with temperature changes in the shells. On the other hand, shells are usually physically affected by various loads such as static loading or excitation due to external dynamic loads. The study of the behavior and static model of shells can be an important field of application in the design of structures. Therefore, by considering the changes in temperature and humidity of the environment, a static load was also applied to the problem. Then, the governing differential

equations were simulated assuming different abutment conditions and transformed into a nonlinear system of algebraic equation using a semi analytical method. Finally, the algebraic equations were solved using the Newton-Raphson method. We tested the correctness of the solution method with the help of FEM commercial software. The effect of changing various parameters including temperature, humidity, shell thickness, external static load, etc. on the elastic behavior of the shells was studied. Most importantly, the behavior of the shells was compared under the same conditions.

2. Geometrical definition

In this research, the governing equations of shell structures with any desired cross-section are extracted and the results are obtained numerically for the stresses created in the structure as well as the resulting deformations. As mentioned, the cross-section of the shell structure can be selected as desired, and with a single set of partial differential equations, each geometrical shape of the shell structure can be mechanically modeled. Therefore, this research is very instructive and due to the fact that there is no limit in the type of geometry, the proposed formulation can be considered for use by other researchers working in the field of mechanical analysis of shell structures. The cross-section of the geometric structure of the studied shell is a function in the form of $z = f(r)$ which will rotate around the z axis. The rotation angle can change up to 360 degrees. Fig. 1 shows the geometric structure studied in this research.

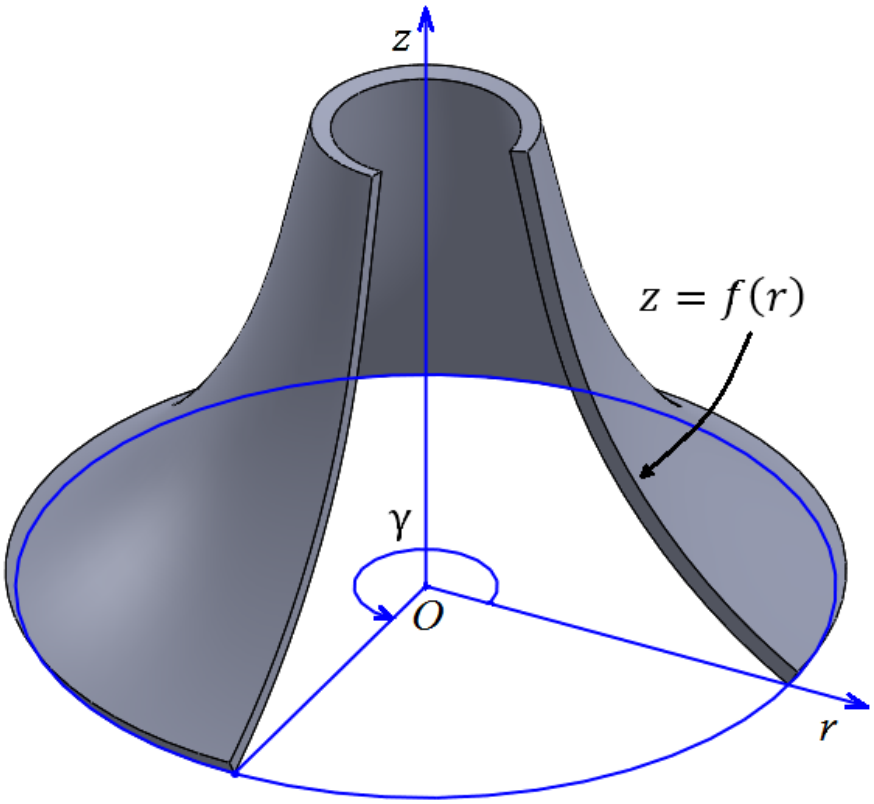

Fig. 1. Structure created by rotation of a profile $z = f(r)$ around z axis $0 < \gamma \leq 360^{\circ}$

According to Fig. 1, $f(r)$ determines the final shape of the shell structure. For example, if $f(r)$ is chosen so that $r = k$ (k is a constant number), the final obtained structure will be a cylindrical structure with a radius of rotation $R = k$. Fig. 2 shows the structure of these cylinders. Also, if the function $f(r)$ represents a straight line, the resulting structure will be a complete or frustum cone structure (Fig. 3). The angle γ can be calculated as $\gamma = \tan\left(\frac{r_2 - r_1}{z_1}\right)$.

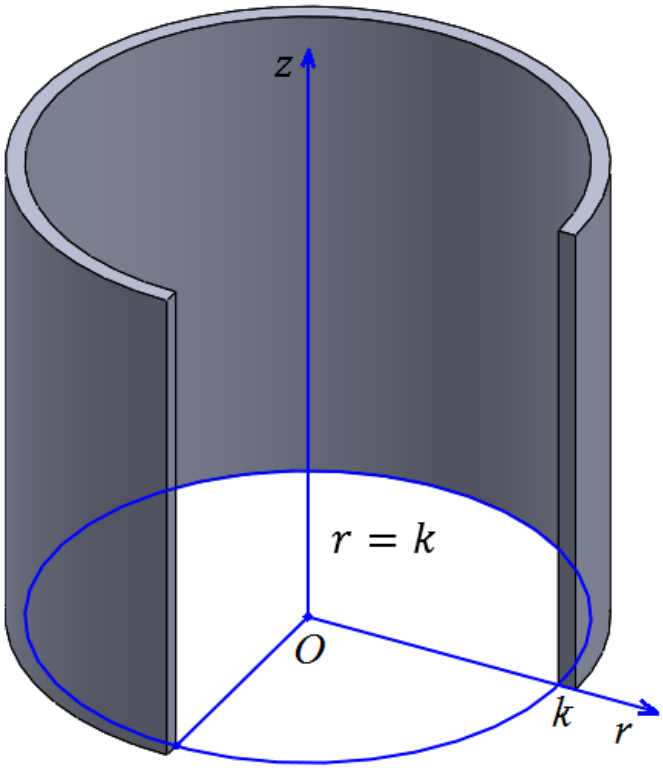

Fig. 2. Cylindrical structure by considering the cross-section function as $r = k$ in which k is an arbitrary constant real number

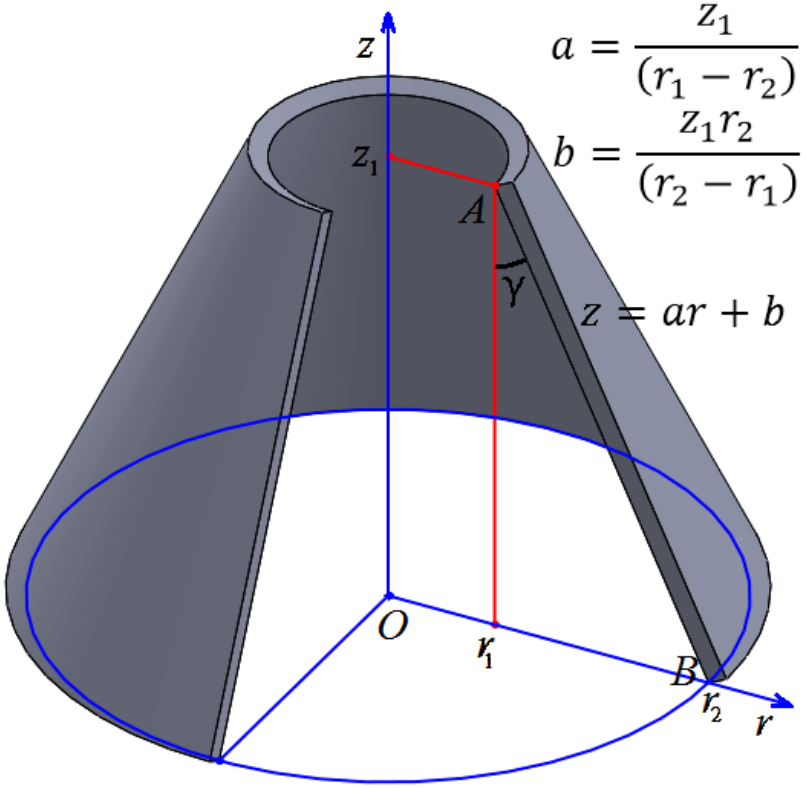

Fig. 3. Frustum cone structure by considering the cross-section function as $f(r) = \left(\frac{z_1}{(r_1 - r_2)}\right) r + \left(\frac{z_1 r_2}{(r_2 - r_1)}\right)$

Therefore, it is observed that a very wide range of shell structures (even spherical and elliptical structures) can be modeled in this way. For example, in spherical and elliptical structures the value of $f(r)$ is equal to $\sqrt{R^2 - r^2}$ and $\left(\frac{b}{a}\right)\sqrt{a^2 - r^2}$ respectively where R, a and b are the radius of the sphere, major and minor axis of the ellipse (Figs. 4 and 5).

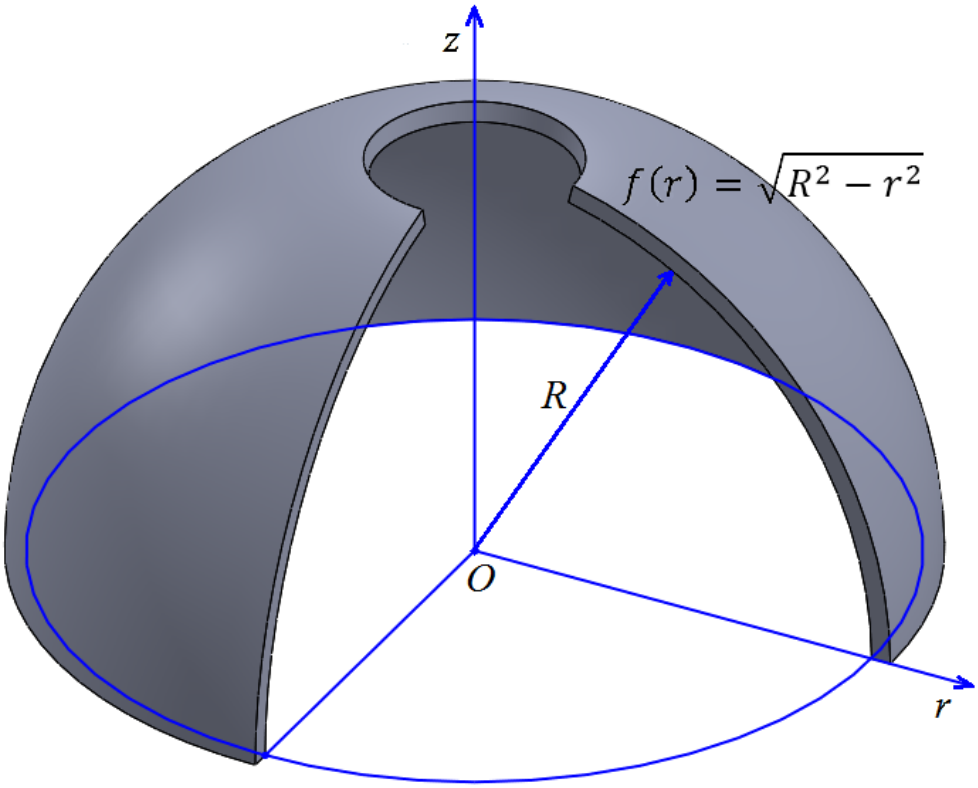

Fig. 4. Spherical structure by considering the cross-section function as $f(r) = \sqrt{R^2 - r^2}$

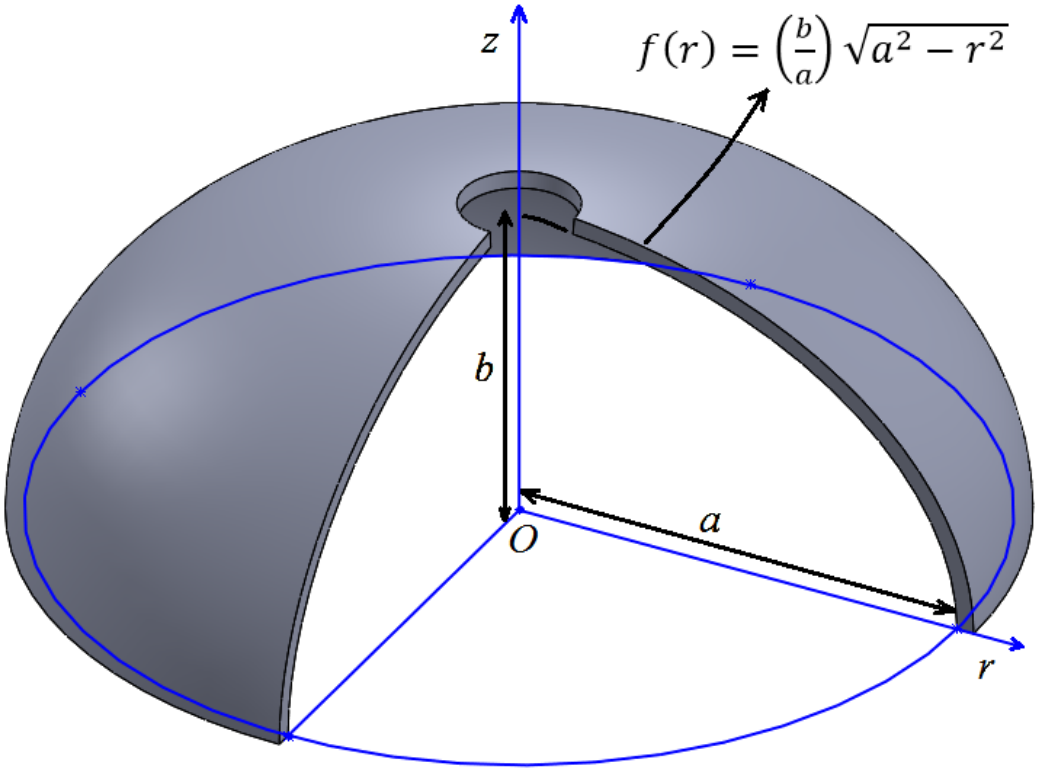

Fig. 5. Elliptical structure by considering the cross-section function as $f(r) = \left(\frac{b}{a}\right)\sqrt{a^2 - r^2}$

The general conclusion is that according to the present study, a large number of structures with different geometries can be studied practically and with just one formulation. Factors such as environmental influences (temperature and humidity), material type (hyper-elastic, viscoelastic or FGM composite) and type of loading can be considered in the extraction steps of the governing equations. Even the effects of small-scale analysis on micro- and nano-structures can be examined after extracting the original equations. The introduced model can be very practical and will be very comprehensive, regardless of the type of analysis. For example, by making changes in the obtained equations from this method (as mentioned earlier) small-scale analysis can also be considered. In this regard, further discussion will be done. A very practical problem could be the analysis of a cooling tower in power plant systems that usually have an exponential cross-section. If there is a cooling tower, the main question is whether the

materials used in it, which can be ordinary composite materials or even a functionally graded materials (FGM), will be able to withstand the weight of the structure or not? (Fig. 6).

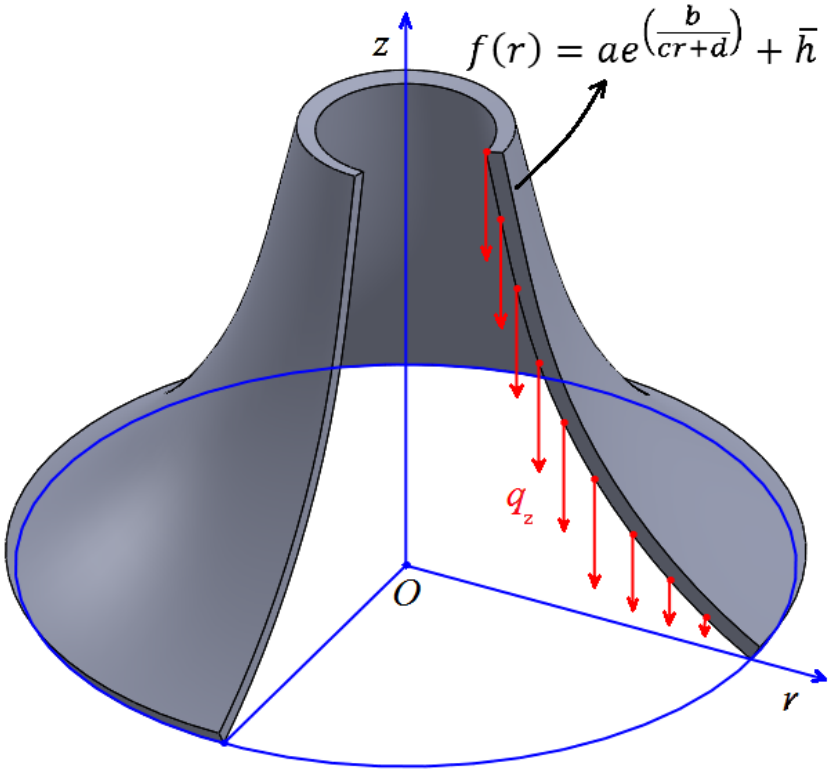

Fig. 6. Geometry of a cooling tower with exponential cross-section under its own weight q_z

Also, in the section on extracting the governing equations, it will be stated that the obtained equations have been extracted in a completely dynamic way. Therefore, the introduced equations have a very high generality for modeling mechanical phenomena.

3. Mathematical modeling of shell with desired cross-section

A cross-section is assumed as the function $z = f(r)$ that revolves around the z axis with a definite γ angle (Fig. 1 shows this section). The thickness of the structure is equal to h. Two conditions can be considered to apply the thickness h.

1. The thickness h is assumed to be constant along the axis r. In this case, the function $h(r)$, which indicates the thickness of the structure in the direction r, will be constant and equal to h_r. For a better and clearer expression of this issue, Fig. 7 is presented.

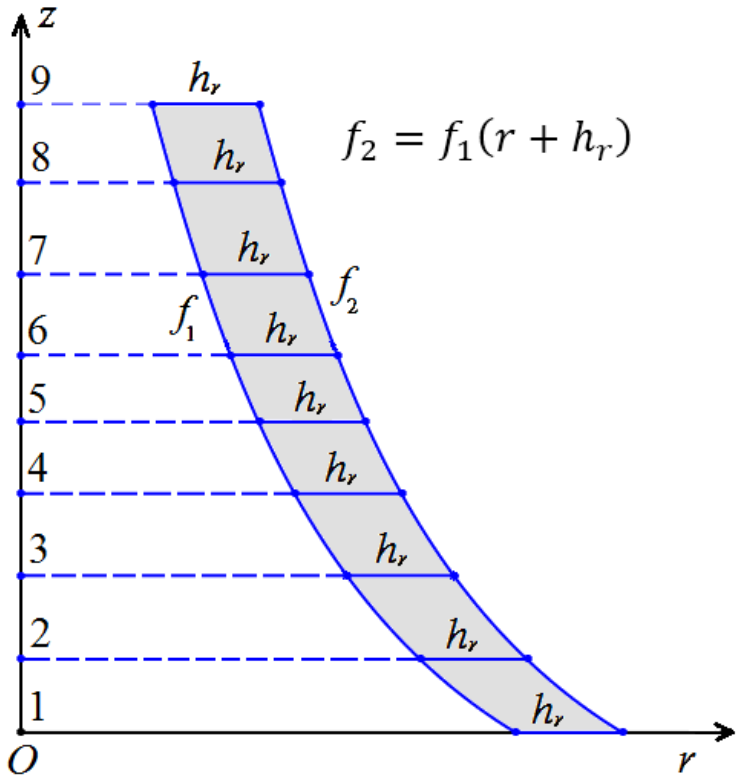

Fig. 7. Thickness of cross-section in condition one

2. Since the cross-section of the structure is presented as a curve $z = f(r)$, it is considered that the thickness of the structure in the direction n (normal and perpendicular to the cross-section) is not constant. According to Fig. 8, as there is an increase in the z direction, the thickness of the structure increases to n. The amount of mentioned increase also depends on the cross-sectional curvature of the structure. In other words, the smaller the slope of the cross-sectional curve, the lower the normal thickness (perpendicular) in that area. For the maximum slope (vertical structure or parallel to the z-axis) the thickness in the r direction will be equal to the thickness of n direction.

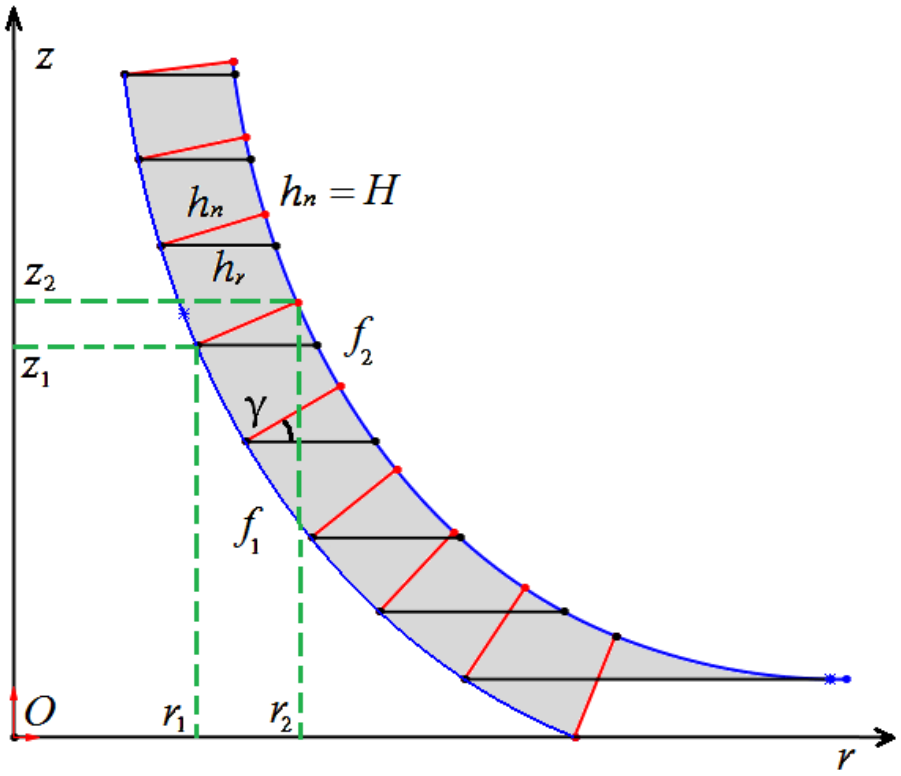

Fig. 8. Thickness of cross-section in condition two

If the cross-section of the structure is considered as a straight line (the geometry of the structure is conical), the thickness in the *n* direction will be equal in all parts of the structure. As a result, there will be a general relationship between thickness h_r (thickness in the direction of r) and thickness h_n (thickness in the direction of *n*), which can be obtained according to Fig. 9 as the following equation.

$$h_n = \frac{h_r}{\cos\gamma} \tag{1}$$

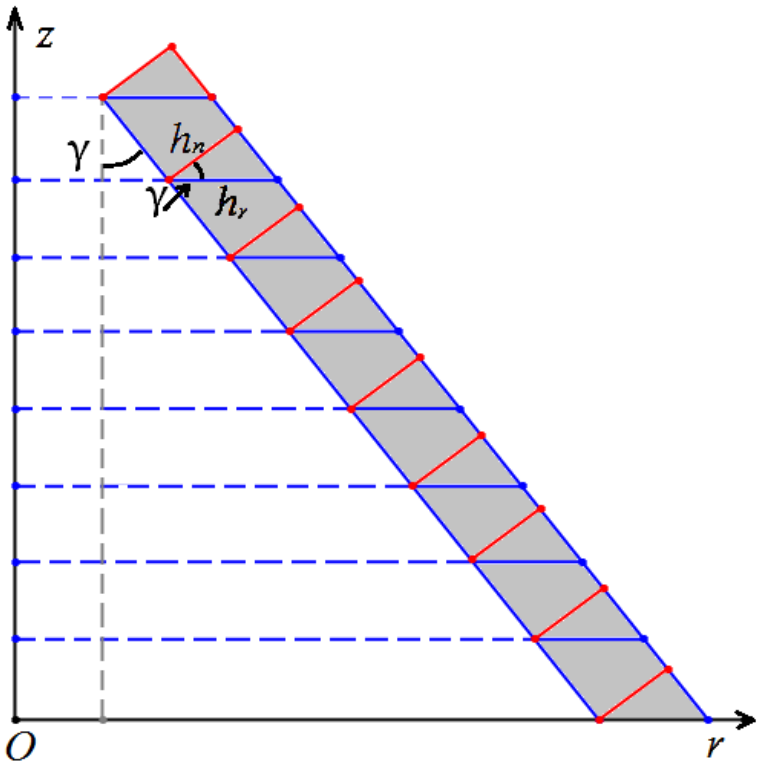

Fig. 9. Thickness of frustum conical structure

But in general, if the cross-section of the structure is curved (condition 2), to obtain the function h_n in the direction of r, or, in other words, $h_n(r)$ is done in details as follows.

According to Fig. 8, the function f_1 represents the relationship between z and r or represents the shape of the cross-sectional curve that is arbitrarily assumed. The function f_2 can be obtained given that the curve f_1 is transferred in the direction n with a constant thickness H. The method of calculating f_2 is that a desired point (for example point A) with coordinates r_1 and z_1 on the curve f_1 is considered. The slope of the line perpendicular to this point can be obtained as the following equation.

$$S_t = \frac{df_1}{dr}, S_p = -\frac{1}{\left(\frac{df_1}{dr}\right)} \tag{2}$$

In the above relation S_t is the slope of the tangent line and S_p is the slope of the line perpendicular to the curve f_1. The coordinates r_1 and z_1 of point A on the curve f_1 can now be calculated on the curve f_2 with the slope of the line S_p.

$$r_2 = r_1 \pm \frac{H\left(\frac{df_1}{dr}\right)}{\sqrt{1+\left(\frac{df_1}{dr}\right)^2}}, z_2 = z_1 \pm \frac{H}{\sqrt{1+\left(\frac{df_1}{dr}\right)^2}} \tag{3}$$

Therefore, the f_2 curve can be defined with respect to the f_1 curve, in which r and z are transferred according to the equations introduced above. Also, the horizontal distance between the two curves f_1. and f_2, which represents $h_n(r)$, can be defined at any point by the value of $\pm\frac{H\left(\frac{df_1}{dr}\right)}{\sqrt{1+\left(\frac{df_1}{dr}\right)^2}}$. The positive and negative signs ($\pm$) for $h_n(r)$ function represent the geometric location of f_2 curve on both sides of f_1 curve.

4. Extraction of the governing equations of the desired shell structure

In the previous section, the geometrical equations of the shell structure with the desired cross-section were expressed. Hereafter, strain field, stress tensor, and the final mechanical governing equations will be formulated.

A rotating shell structure with a functional cross-section ($z = f(r)$) is considered in the hygro-thermal environment as shown in Fig. 10. The structure rotates around the z-axis with constant angular velocity ω as $\omega = \frac{d\theta}{dt}$. It means that there is not any angular acceleration and $\alpha = \frac{d\omega}{dt} = 0$.

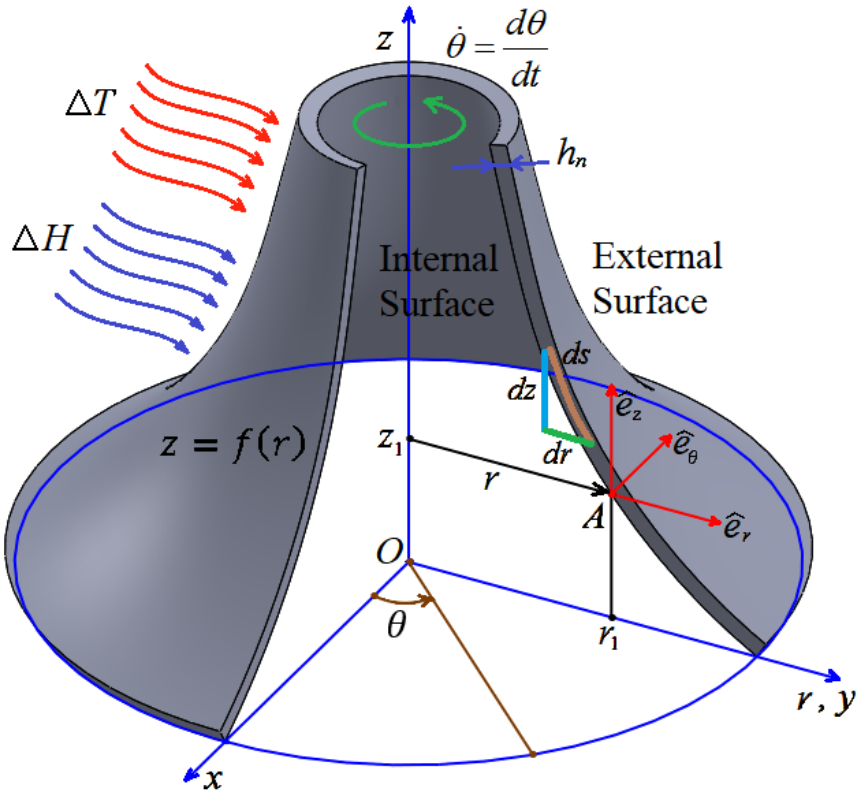

Fig. 10. Schematic view of a rotating shell structure with functional cross-section shape $z = f(r)$ in hygro-thermal environment

As shown in Fig. 10, the geometric location of point A on the shell can be introduced using the definition of a cylindrical coordinate system as the following equations.

$$\begin{cases} x = r\cos\theta \\ y = r\sin\theta \\ z = z \end{cases} \tag{4}$$

It should be noted that here the radius r is no longer constant, unlike a cylinder whose cross-sectional radius is constant and equal to R. The value of r will change in the z direction. If the function $z = f(r)$ is considered, it is sufficient to obtain the changes r relative to z by calculating the inverse of the function $f(r)$ to obtain the function $r = f(z)$. The volume differential according to Fig. 10 can be written as $dV = rd\theta drdz$ where $r = f(z)$. As a result, the volume differential will be $dV = f(z)d\theta drdz$.

The governing equations are now derived from a cylindrical coordinate system in which the radius of the cylinder is no longer constant and follows the function $r = f(z)$. The strain field has been obtained before in a cylindrical coordinate system with $\vec{\nabla}\vec{U}$ definition in which the vector of $\vec{U}$ is the displacement vector as $\vec{U} = U_r\hat{e}_r + U_\theta\hat{e}_\theta + U_z\hat{e}_z$ [82]. Therefore, by defining the strain tensor as a matrix equation, the strain components can be obtained in the new cylindrical coordinate system.

$$\vec{\vec{\varepsilon}} = \frac{1}{2}\left[\vec{\nabla}\vec{U} + \left(\vec{\nabla}\vec{U}\right)^T + \vec{\nabla}\vec{U}\cdot\left(\vec{\nabla}\vec{U}\right)^T\right] \tag{5}$$

$$\vec{\nabla}\vec{U} = \begin{bmatrix}\frac{\partial}{\partial r}\hat{e}_r & \frac{1}{r}\frac{\partial}{\partial\theta}\hat{e}_\theta & \frac{\partial}{\partial z}\hat{e}_z\end{bmatrix}\begin{bmatrix}U_r\hat{e}_r\\ U_\theta\hat{e}_\theta\\ U_z\hat{e}_z\end{bmatrix} = \begin{bmatrix}\frac{\partial U_r}{\partial r} & \frac{\partial U_\theta}{\partial r} & \frac{\partial U_z}{\partial r}\\ \frac{1}{r}\left(\frac{\partial U_r}{\partial\theta} - U_\theta\right) & \frac{1}{r}\left(\frac{\partial U_\theta}{\partial\theta} + U_r\right) & \frac{1}{r}\frac{\partial U_z}{\partial\theta}\\ \frac{\partial U_r}{\partial z} & \frac{\partial U_\theta}{\partial z} & \frac{\partial U_z}{\partial z}\end{bmatrix}$$

$$\vec{\vec{\varepsilon}}_{ij} = \begin{bmatrix}\varepsilon_{rr} & \varepsilon_{r\theta} & \varepsilon_{rz}\\ \varepsilon_{\theta r} & \varepsilon_{\theta\theta} & \varepsilon_{\theta z}\\ \varepsilon_{zr} & \varepsilon_{z\theta} & \varepsilon_{zz}\end{bmatrix} - (\alpha_T\Delta T + \beta_H\Delta H)\begin{bmatrix}1 & 0 & 0\\ 0 & 1 & 0\\ 0 & 0 & 1\end{bmatrix} \tag{6}$$

$$\varepsilon_{rr} = \left(\frac{\partial U_r}{\partial r}\right) + \frac{1}{2}\left(\frac{\partial U_r}{\partial r}\right)^2 \qquad 2\varepsilon_{r\theta} = 2\varepsilon_{\theta r} = \frac{1}{r}\left(\frac{\partial U_r}{\partial\theta} - U_\theta\right) + \left(\frac{\partial U_\theta}{\partial r}\right) + \frac{1}{r}\left(\frac{\partial U_r}{\partial r}\right)\left(\frac{\partial U_r}{\partial\theta}\right)$$

$$2\varepsilon_{rz} = 2\varepsilon_{zr} = \left(\frac{\partial U_r}{\partial z} + \frac{\partial U_z}{\partial r}\right) \qquad \varepsilon_{\theta\theta} = \frac{1}{r}\left(\frac{\partial U_\theta}{\partial\theta} + U_r\right) + \frac{1}{2r^2}\left(\left(\frac{\partial U_r}{\partial\theta}\right)^2 + U_r^2\right)$$

$$2\varepsilon_{\theta z} = 2\varepsilon_{z\theta} = \frac{1}{r}\frac{\partial U_z}{\partial\theta} + \frac{\partial U_\theta}{\partial z} \qquad \varepsilon_{zz} = \frac{\partial U_z}{\partial z}$$

In the above equations, $\vec{\vec{\varepsilon}}$ is the strain tensor and $\left(\vec{\nabla}\vec{U}\right)^T$ is the transposed of the $\vec{\nabla}\vec{U}$ matrix. α_T and β_H are the thermal expansion and moisture coefficients. The environment temperature and humidity differences are expressed by ΔT and ΔH. By considering the Hook stress law ($\vec{\vec{\sigma}}_{ij} = C:\vec{\vec{\varepsilon}}_{ij}$), the values of structural stresses in the new cylindrical coordinate system will be obtained by defining the function $r = f(z)$. The matrix C is the elastic stiffness characteristic of the structure material, which is introduced as the following matrix.

$$C = \frac{E(r)}{1-(\nu(\bar{r}))^2}\begin{bmatrix} 1 & \nu(r) & 0 & 0 & 0 & 0 \\ \nu(r) & 1 & 0 & 0 & 0 & 0 \\ 0 & 0 & \frac{1-\nu(r)}{2} & 0 & 0 & 0 \\ 0 & 0 & 0 & \frac{1-\nu(r)}{2} & 0 & 0 \\ 0 & 0 & 0 & 0 & \frac{1-\nu(r)}{2} & 0 \\ 0 & 0 & 0 & 0 & 0 & \frac{1-\nu(r)}{2} \end{bmatrix} \tag{7}$$

In matrix C, E and ν are Young's elasticity modulus and Poisson's ratio coefficient that varies along the thickness direction. In other words, the structure material in this study is considered as functionally graded material (FGM). The definition of $E(\bar{r})$ and $\nu(\bar{r})$ can be given by the following equations [83–86].

$$E(r) = (E_1 - E_2)\left(\frac{r}{h}+\frac{1}{2}\right)^{\zeta} + E_2; \nu(r) = (\nu_1 - \nu_2)\left(\frac{r}{h}+\frac{1}{2}\right)^{\zeta} + \nu_2 \quad \left(-\frac{h}{2} \le r \le \frac{h}{2}\right) \tag{8}$$

In the above equations E_1 and ν_1 are Young's elasticity modulus and Poisson's ratio coefficient on the inner surface of the structure. Also, E_2 and ν_2 are mentioned values on the outer surface of the structure according to Fig. 10. Parameter ζ represents the intensity of slope variations from internal to external material characterizations.

In this research, the principle of minimum potential energy has been used to derive the governing equations and boundary conditions as the following general relation.

$$\delta\Pi = \delta P_\varepsilon + \delta P_f + \delta P_{k_1} + \delta P_{k_2} = 0 \tag{9}$$

$$\delta P_\varepsilon = \int_0^t \left(\iiint_V \sigma_{ij}\delta\varepsilon_{ij} dV\right) dt \quad i,j = r,\theta,z \quad \text{(V is the volume)}$$

$$\delta P_f = -\int_0^t \left(\iiint_V (q_r\delta U_r + q_\theta \delta U_\theta + q_z \delta U_z) dV\right) dt$$

$$\delta P_{k_1} = -\frac{\delta}{2}\int_0^t \left(\iiint_V \rho\left(\left(\frac{\partial U_r}{\partial t}\right)^2 + \left(\frac{\partial U_\theta}{\partial t}\right)^2 + \left(\frac{\partial U_z}{\partial t}\right)^2\right) dV\right) dt$$

$$\delta P_{k_2} = -\int_0^t \left(\iiint_v -\rho r(\dot{\theta}^2)\delta U_r dV \right) dt$$

In the above equation, P_ε, P_f, P_{k_1} and P_{k_2} are the strain energy changes, the energy changes due to the application of external loads on the shell, the kinetic energy changes, and the energy changes due to the dynamic motion of the structure (in case of dynamic motion of the structure), respectively. According to Fig. 10, the volume and area differential dV and dA are calculated as follows:

$$dA = rd\theta ds, dV = rd\theta ds dr \tag{10}$$

$$(ds)^2 = (dz)^2 + (dr)^2 = (dz)^2\left(1 + \left(\frac{dr}{dz}\right)^2\right) \rightarrow ds = \left(\sqrt{\left(1 + \left(\frac{dr}{dz}\right)^2\right)}\right) dz, \tag{11}$$

The cross-section profile follows the function $z = f(r)$. Consequently, it can be possible to calculate $r = g(z)$ in which g is the inverse of function f as $g(z) = f^{-1}$. As a result, dA and dV will be reformulated in below:

$$dA = r\left(\sqrt{\left(1 + \left(\frac{dg(z)}{dz}\right)^2\right)}\right) dz d\theta, dV = r\left(\sqrt{\left(1 + \left(\frac{dg(z)}{dz}\right)^2\right)}\right) dz d\theta dr, y(z) =$$

$$\sqrt{\left(1 + \left(\frac{dg(z)}{dz}\right)^2\right)} \rightarrow dA = ry(z) dz d\theta, dV = ry(z) dz d\theta dr \tag{12}$$

The expansion of P_ε, P_f, P_{k_1} and P_{k_2} in Eq. (9) are presented below:

$$\delta P_\varepsilon = \int_0^t (\iiint_V (\sigma_{rr}\delta\varepsilon_{rr} + \sigma_{r\theta}\delta\varepsilon_{r\theta} + \sigma_{rz}\delta\varepsilon_{rz} + \sigma_{\theta r}\delta\varepsilon_{\theta r} + \sigma_{\theta\theta}\delta\varepsilon_{\theta\theta} + \sigma_{\theta z}\delta\varepsilon_{\theta z} + \sigma_{zr}\delta\varepsilon_{zr} +$$

$$\sigma_{z\theta}\delta\varepsilon_{z\theta} + \sigma_{zz}\delta\varepsilon_{zz}) dV) dt = \int_0^t (\iiint_V (\sigma_{rr}\delta\varepsilon_{rr} + \sigma_{zz}\delta\varepsilon_{zz} + \sigma_{\theta\theta}\delta\varepsilon_{\theta\theta} + 2\sigma_{r\theta}\delta\varepsilon_{r\theta} + 2\sigma_{rz}\delta\varepsilon_{rz} +$$

$$2\sigma_{\theta z}\delta\varepsilon_{\theta z}) dV) dt = \int_0^t \left(\iiint_V \left(\sigma_{rr} ry(z) \left(\left(\frac{\partial \delta U_r}{\partial r}\right) + \left(\frac{\partial U_r}{\partial r}\right)\left(\frac{\partial \delta U_r}{\partial r}\right) \right) + \sigma_{zz} ry(z) \left(\frac{\partial \delta U_z}{\partial z}\right) + \right.\right.$$

$$\left.\left. \sigma_{\theta\theta} y(z) \left(\left(\frac{\partial \delta U_\theta}{\partial \theta} + \delta U_r\right) + \frac{1}{r}\left(\left(\frac{\partial U_r}{\partial \theta}\right)\left(\frac{\partial \delta U_r}{\partial \theta}\right) + U_r \delta U_r \right) \right) + \sigma_{r\theta} y(z) \left(\left(\frac{\partial \delta U_r}{\partial \theta} - \delta U_\theta\right) + r\left(\frac{\partial \delta U_\theta}{\partial r}\right) + \right.\right.$$

$$\left(\left(\frac{\partial U_r}{\partial r}\right)\left(\frac{\partial \delta U_r}{\partial \theta}\right)+\left(\frac{\partial \delta U_r}{\partial r}\right)\left(\frac{\partial U_r}{\partial \theta}\right)\right)\Big)+\sigma_{rz}ry(z)\left(\frac{\partial \delta U_r}{\partial z}+\frac{\partial \delta U_z}{\partial r}\right)+\sigma_{\theta z}y(z)\left(\frac{\partial \delta U_z}{\partial \theta}+r\frac{\partial \delta U_\theta}{\partial z}\right)\Big)dzd\theta dr\Big)dt$$

(13)

$$\delta P_f=\int_0^t\left(\iiint_V(q_r\delta U_r+q_\theta\delta U_\theta+q_z\delta U_z)g(z)y(z)dzd\theta dr\right)dt \quad (14)$$

$$\delta P_{k_1}=-\frac{\delta}{2}\int_0^t\left(\iiint_V\rho\left(\left(\frac{\partial U_r}{\partial t}\right)^2+\left(\frac{\partial U_\theta}{\partial t}\right)^2+\left(\frac{\partial U_z}{\partial t}\right)^2\right)dV\right)dt=-\int_0^t\left(\iiint_V\rho\left(\left(\frac{\partial U_r}{\partial t}\frac{\partial \delta U_r}{\partial t}\right)+\right.\right.$$

$$\left.\left.\left(\frac{\partial U_\theta}{\partial t}\frac{\partial \delta U_\theta}{\partial t}\right)+\left(\frac{\partial U_z}{\partial t}\frac{\partial \delta U_z}{\partial t}\right)\right)g(z)y(z)dzd\theta dr\right)dt \quad (15)$$

$$\delta P_{k_2}=-\int_0^t\left(\iiint_v-\rho r\left(\dot{\theta}^2\right)\delta U_r g(z)y(z)dzd\theta dr\right)dt \quad (16)$$

According to the stationary principle of minimum potential energy, potential energy variations should be equal to zero. Finally, by summing the effects of $\delta U_r, \delta U_\theta$ and δU_z variables, the dynamic governing equations of the shell structure with functional cross-section can be introduced as the following 3 equations.

$$\delta U_r: g(z)y(z)\frac{\partial \sigma_{rr}}{\partial r}+y(z)\frac{\partial \sigma_{r\theta}}{\partial \theta}+\frac{\partial}{\partial z}(g(z)y(z)\sigma_{rz})+y(z)(\sigma_{rr}-\sigma_{\theta\theta})+g(z)y(z)q_r=$$

$$g(z)y(z)\rho\frac{\partial^2 U_r}{\partial t^2}-\left(g(z)\right)^2y(z)\rho\omega^2 \quad (17)$$

$$\delta U_\theta: g(z)y(z)\frac{\partial \sigma_{r\theta}}{\partial r}+y(z)\frac{\partial \sigma_{\theta\theta}}{\partial \theta}+\frac{\partial}{\partial z}(g(z)y(z)\sigma_{\theta z})+2y(z)\sigma_{r\theta}+g(z)y(z)q_\theta=$$

$$g(z)y(z)\rho\frac{\partial^2 U_\theta}{\partial t^2} \quad (18)$$

$$\delta U_z: g(z)y(z)\frac{\partial \sigma_{rz}}{\partial r}+y(z)\frac{\partial \sigma_{\theta z}}{\partial \theta}+\frac{\partial}{\partial z}(g(z)y(z)\sigma_{zz})+y(z)\sigma_{rz}+g(z)y(z)q_z=$$

$$g(z)y(z)\rho\frac{\partial^2 U_z}{\partial t^2} \quad (19)$$

The above partial differential equations give three-dimensional results. Although the introduced equations provide accurate 3D results, solving the above equation system itself is a big challenge. Also, for structures whose thickness is smaller than other dimensions (even for moderately thick structures), there is no need to use 3D analysis, and often plate and shell

theories are used, which provide relatively accurate results with a very good approximation. In these theories, it is assumed that the strain variations through the thickness are negligible ($\varepsilon_{rr} = 0$). As can be seen, the displacement vector $\vec{U}$ is general and any kind of displacement field can be used in the above equations. In this research, the first-order shear deformation theory (FSDT) has been utilized to analyze the shell structure with any desired cross-section. FSDT displacement field is considered because of its efficiency and obtaining appropriate results with simple formulation has already been proven by many researchers [54, 77 and 82]. But as mentioned before, any kind of displacement field can be used in strain equations. The displacement field of FSDT for the $\vec{U}$ vector is given by the following equations.

$$\begin{cases} U_\theta(\bar{r},\theta,z,t) = u_0(\theta,z,t) + r\psi_1(\theta,z,t) \\ U_z(\bar{r},\theta,z,t) = v_0(\theta,z,t) + r\psi_2(\theta,z,t) \\ U_r(\bar{r},\theta,z,t) = w_0(\theta,z,t) \end{cases} \tag{20}$$

In the above equations u_0, v_0, w_0 are the transfer displacement functions. ψ_1 and ψ_2 are the rotation functions around the z and θ axes, respectively. By repeating the computational process similar to the previous case (extraction of Eqs. (17–19)) and using the principle of minimum potential energy, the 5 governing equations based on FSDT theory will be obtained as follows:

$$\delta u_0: y(z)N_{r\theta} + y(z)\frac{\partial N_{\theta\theta}}{\partial\theta} + \frac{\partial}{\partial z}(g(z)y(z)N_{z\theta}) - g(z)y(z)\left(I_1\frac{\partial^2 u_0}{\partial t^2} + I_2\frac{\partial^2\psi_1}{\partial t^2}\right) = 0 \tag{21}$$

$$\delta v_0: y(z)\frac{\partial N_{z\theta}}{\partial\theta} + \frac{\partial}{\partial z}(g(z)y(z)N_{zz}) - g(z)y(z)\left(I_1\frac{\partial^2 v_0}{\partial t^2} + I_2\frac{\partial^2\psi_2}{\partial t^2}\right) = 0 \tag{22}$$

$$\delta w_0: y(z)\frac{\partial N_{r\theta}}{\partial\theta} - y(z)N_{\theta\theta} + \frac{\partial}{\partial z}(g(z)y(z)N_{rz}) + \frac{y(z)}{g(z)}\frac{\partial}{\partial\theta}\left(N_{\theta\theta}\frac{\partial w_0}{\partial\theta}\right) - \frac{y(z)}{g(z)}(N_{\theta\theta}w_0) +$$
$$y(z)\frac{\partial}{\partial\theta}\left(N_{z\theta}\frac{\partial w_0}{\partial z}\right) + \frac{\partial}{\partial z}\left(y(z)N_{z\theta}\frac{\partial w_0}{\partial\theta}\right) + \frac{\partial}{\partial z}\left(g(z)y(z)N_{zz}\frac{\partial w_0}{\partial z}\right) + g(z)y(z)q_r -$$
$$I_1\big(g(z)\big)^2 y(z)\omega^2 - I_1 g(z)y(z)\frac{\partial^2 w_0}{\partial t^2} = 0 \tag{23}$$

$$\delta\psi_1: y(z)M_{r\theta} - g(z)y(z)N_{r\theta} + y(z)\frac{\partial M_{\theta\theta}}{\partial\theta} + \frac{\partial}{\partial z}(g(z)y(z)M_{z\theta}) - g(z)y(z)\left(I_2\frac{\partial^2 u_0}{\partial t^2} + I_3\frac{\partial^2\psi_1}{\partial t^2}\right) = 0 \quad (24)$$

$$\delta\psi_2: y(z)\frac{\partial M_{z\theta}}{\partial\theta} - g(z)y(z)N_{rz} + \frac{\partial}{\partial z}(g(z)y(z)M_{zz}) - g(z)y(z)\left(I_2\frac{\partial^2 v_0}{\partial t^2} + I_3\frac{\partial^2\psi_2}{\partial t^2}\right) = 0 \quad (25)$$

The definition of stress and moment resultants (N_{ij} and M_{ij} $(i,j = r,\theta,z)$) and also moment of inertia I_i $(i = 1..3)$ in above equations are presented below.

$$\begin{cases} (N_{zz}, N_{z\theta}, N_{\theta\theta}, N_{r\theta}, N_{rz}) = \int_{-\frac{h}{2}}^{\frac{h}{2}} (\sigma_{zz}, \sigma_{z\theta}, \sigma_{\theta\theta}, \sigma_{r\theta}, \sigma_{rz})dr \\ (M_{zz}, M_{z\theta}, M_{\theta\theta}, M_{r\theta}) = \int_{-\frac{h}{2}}^{\frac{h}{2}} (\sigma_{zz}, \sigma_{z\theta}, \sigma_{\theta\theta}, \sigma_{r\theta})rdr \\ (I_1, I_2, I_3) = \int_{-\frac{h}{2}}^{\frac{h}{2}} \rho(1, r, r^2)dr \end{cases} \quad (26)$$

The obtained dynamic governing equations have been solved by using SAPM method. The details for SAPM method can be studied in many references [2–3 and 5]. Applying SAPM method is very simple and gives accurate results. There are so many advantages that the authors decided to use this methodology for solving the set of governing equations (Eqs. (21–25)).

5. Numerical results

5.1. Validation of the results

First of all, the results obtained from the presented formulation should be validated and compared with the other available literatures. If the formulation and solving methodology are correct, they should give appropriate results. For this purpose, the results of a conical shell structure made of FGM material Al_2O_3 have been compared with the results of reference [87 and 88]. The properties of conical structure can be seen as follow:

$$E_c = 380\ GPa; E_M = 70\ GPa; \nu_c = \nu_M = 0.3; \zeta = 2 \quad (27)$$

The results of normalized central deflection ($\overline{w} = \frac{wh^3E_c}{q_zL^4}$) can be observed in Table 1 for different amounts of angle of the semi-vertex of the cone (α) and the length to thickness ratio (L/h). As it can be observed, the results of present paper are in a good agreement with the results of other references. Consequently, the applied formulation and solution method in this research are reliable and give appropriate results.

Table 1. The normalized central deflection ($\overline{w}$) results of a FGM conical shell under uniform loading

α	L/h	Reference	$\overline{w}$	α	L/h	Reference	$\overline{w}$
11.25°	10	ANSYS [87]	0.0195000	22.5°	10	ANSYS [87]	0.024100
		[87]	0.0196000			[87]	0.0242000
		FSDT [88]	0.0200570			FSDT [88]	0.0247490
		GFSDT [88]	0.0200300			GFSDT [88]	0.0247060
		UTSDT [88]	0.0200300			UTSDT [88]	0.0247140
		GUTSDT [88]	0.0199520			GUTSDT [88]	0.0246710
		Present Paper	0.0200664			Present Paper	0.0247586
	20	ANSYS [87]	0.0088500		20	ANSYS [87]	0.0114000
		[87]	0.0088400			[87]	0.0114000
		FSDT [88]	0.0090231			FSDT [88]	0.0161200
		GFSDT [88]	0.0089951			GFSDT [88]	0.0158400
		UTSDT [88]	0.0090271			UTSDT [88]	0.0161700
		GUTSDT [88]	0.0089991			GUTSDT [88]	0.0158900
		Present Paper	0.0090301			Present Paper	0.0161269
45°	10	ANSYS [87]	0.0354000	60°	10	ANSYS [87]	0.0433000
		[87]	0.0356000			[87]	0.0439000
		FSDT [88]	0.0361210			FSDT [88]	0.0442780
		GFSDT [88]	0.0361080			GFSDT [88]	0.0442810
		UTSDT [88]	0.0361080			UTSDT [88]	0.0443500
		GUTSDT [88]	0.0361190			GUTSDT [88]	0.0443540
		Present Paper	0.0361383			Present Paper	0.0442993
	20	ANSYS [87]	0.0200000		20	ANSYS [87]	0.0297000
		[87]	0.0202000			[87]	0.0300000
		FSDT [88]	0.0203510			FSDT [88]	0.0301270
		GFSDT [88]	0.0203300			GFSDT [88]	0.0301290
		UTSDT [88]	0.0203620			UTSDT [88]	0.0301530
		GUTSDT [88]	0.0203410			GUTSDT [88]	0.0301440
		Present Paper	0.0203616			Present Paper	0.0301404

5.2. Elliptical structure analysis

The material specification for numerical analysis can be seen in Table 2 (stainless steel 304). The material properties for all numerical analyses are the same from now on, however, the geometrical properties are different for each problem and will be mentioned in its own analysis.

Table 2. Material properties of the structure for numerical analysis

Young's elasticity modulus (E) (GPa)	Poisson ratio (ν)	Density (ρ) ($\frac{kg}{m^3}$)	Thermal expansion coefficient (α_T) ($\frac{1}{^\circ C}$)
190	0.29	8000	17.3×10^{-6}

One of the most important advantages of using the equations presented in this research is the analysis of elliptical structures. As mentioned earlier, the section obtained from the revolving of a function can have any desired shape (Fig. 5). If the cross-sectional equation is considered according to the following equation, an ellipse is obtained from the period of the function $f(r)$:

$$\left(\frac{z}{b}\right)^2 + \left(\frac{r}{a}\right)^2 = 1 \tag{28}$$

The geometrical sizes are $a = 1.2m; b = 1m; h = 0.01m$ and the structure under the normal uniform loading as $q_n = 5\ MPa$. The results of the present study and the FEM software can be seen in Figs. 11 and 12 for the resulting deformations and the stresses. As can be seen, the results are in good agreement with the results obtained from the software, which shows the strength of using the analysis presented in this study. Analysis of elliptical structures has always been a great challenge for researchers and it is observed that due to the complex relationships and the presence of elliptic integrals in the obtained equations, simulation and study of elliptical structures is much more complex than other shell structures. However, the comprehensive

equations presented in this study have a good ability for the mechanical analysis of elliptical structures.

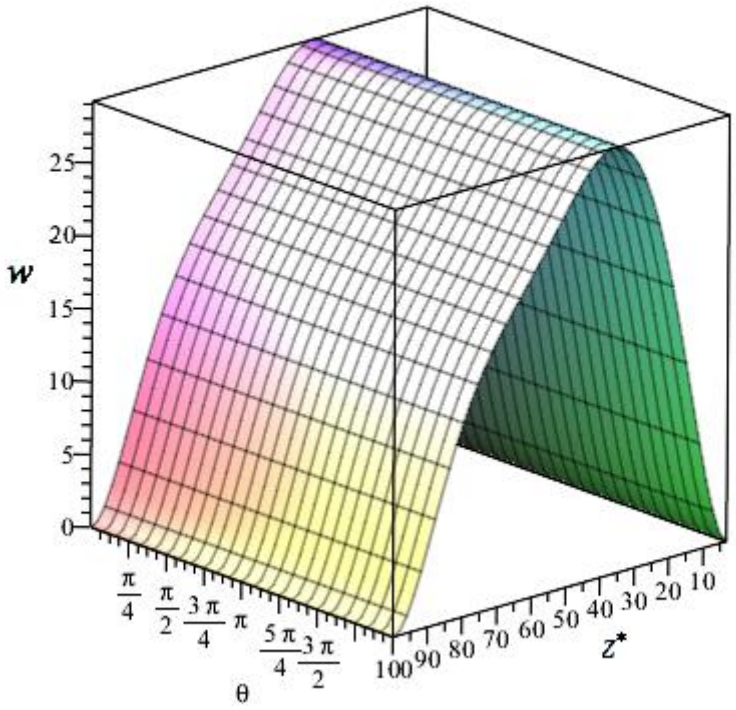

Fig. 11. Deflection results of elliptical shell according to presented analysis in this study

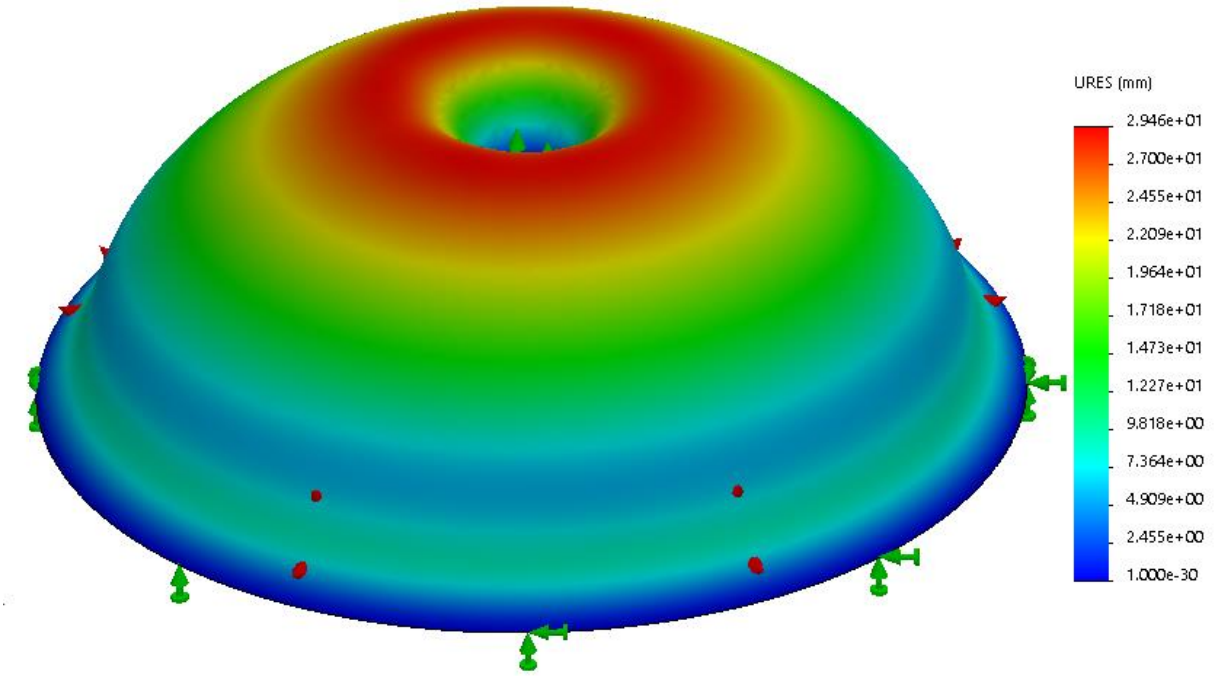

Fig. 12. FEM Software results of elliptical shell

As mentioned before, the analysis of elliptical structure has always been associated with many challenges. In the previous conclusion, a comparison between the results obtained in this study and the software based on FEM was done and the accuracy of the results was discussed. Two other factors influencing the results of an elliptical structure will now be examined. The effect of ambient temperature and rotational speed of the elliptical structure on its deformation and deflection can be seen in two Figs. 13 and 14. The geometrical and material specifications of the structure are the same as Figs. 11 and 12. The horizontal axis of the two graphs in Figs. 13 and 14 is the dimensionless parameter of the size of the elliptical structure (a/b) (Fig. 5). If $a = b$, the elliptical structure will become a spherical structure. The farther the value of a is from b, the farther the shape of the resulting structure will be from the spherical case, and the greater the geometric asymmetry of the problem.

According to Fig. 13, it is observed that with increasing ambient temperature, the deformation of the structure increases, and also with increasing the dimensionless parameter (a/b), it is observed that the deflection of the structure will increase. The mentioned increase is almost linearly (with a small difference) in exchange for the increase of the parameter (a/b). The slope of the diagram in Fig. 13 will increase with increasing ambient temperature, in other words, the higher the ambient temperature, the greater the effect of increasing the size (a/b) on increasing the deformation of the structure.

Fig. 14 shows the effect of the rotational speed of the elliptical structure with the same conditions as in Fig. 13. Increasing the rotational speed of the structure will also increase the resulting dynamic deformations in the structure. Also, the effect of rotational speed on the high speeds of the structure is more important. It can be seen that according to Fig. 14, as the rotational speed of the structure increases, increasing the size parameter (a/b) will have a

greater effect on the intensity of the increase of deflection results. And the results will have a nonlinearly upward trend.

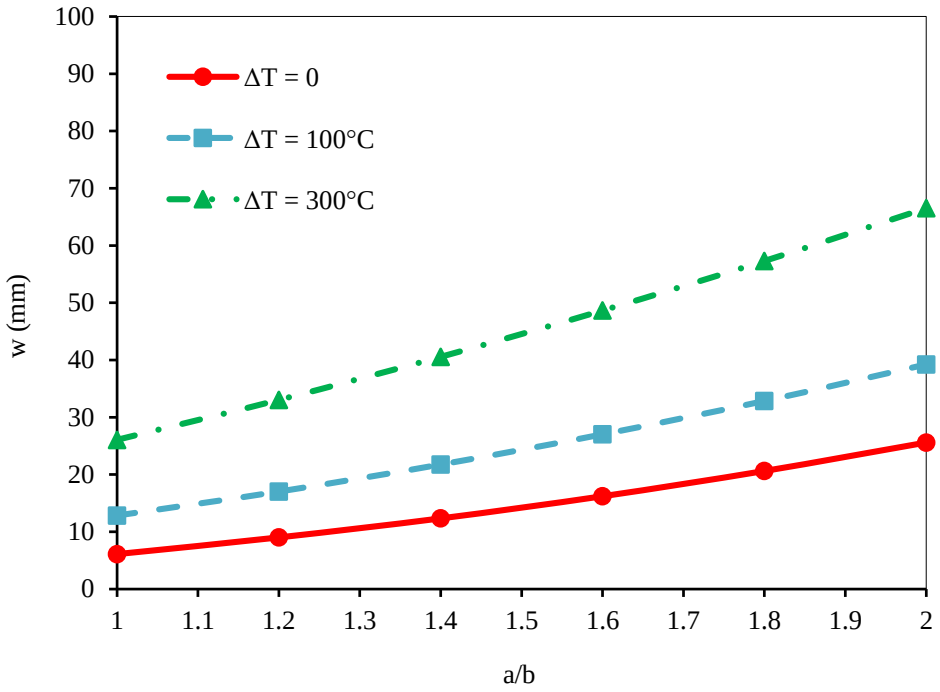

Fig. 13. Deflection results of elliptical structure versus (a/b) parameter for different amounts of ΔT

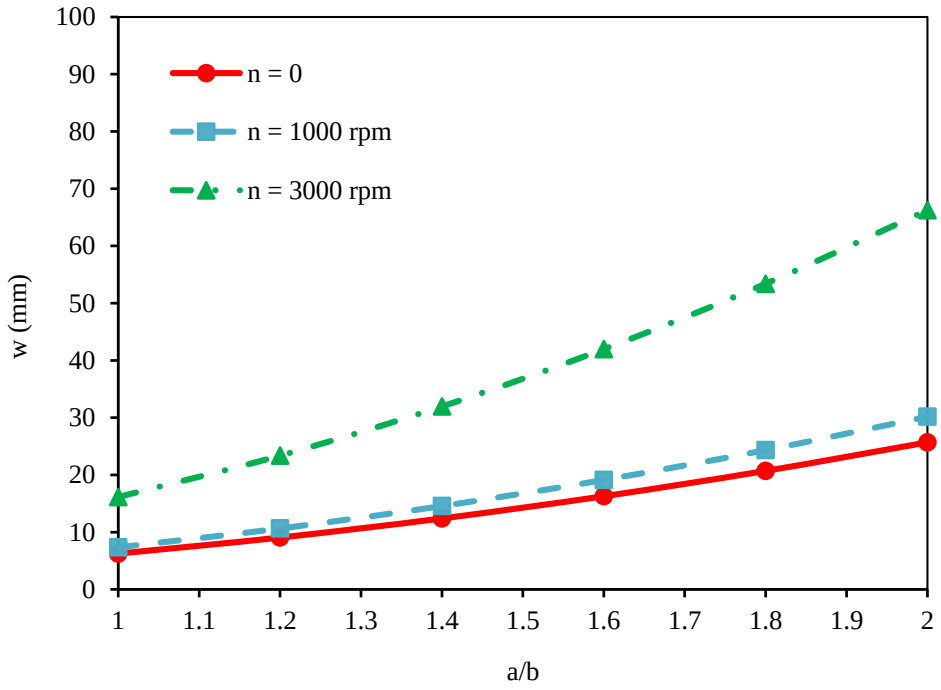

Fig. 14. Effect of angular rotation speed on deflection results of elliptical structure versus (a/b) parameter

More results can be obtained about elliptical structures according to the relationships presented in this study. Due to the comprehensiveness of the basic equations in this research, their use to obtain various results for differentiated elliptical structures and can be a good reference for researchers who study the mechanical behavior of shell structures in different comparisons.

5.3. Analysis of spherical, conical and functional cone structures

In this part, three spherical, conical, and functional cone shell structures will be simulated. The schematic diagram of the three structures and analysis can be seen in Fig. 15. As can be observed, the three structures are common at the beginning and end boundaries and only the type of curve is different between them. The results of the present study can be seen for the deformations in three Figs. 16 to 18 and the von Mises stresses in Figs. 19 to 21. Also, the

results obtained from the software for the three structures analyzed for comparison are shown in Figs. 22 to 27. The radius and thickness of spherical structure is $R = 1m$ and $h = 0.01m$ respectively. The structures are under the uniform transverse loading $q_r = 5\,MPa$. By comparing the results of the analysis presented in this research with the software results, a suitable match between the results can be observed. Other results obtained in this section include that the spherical structure is more resistant among the three structures analyzed. In other words, the farther away from the spherical structure and the closer we get to the functional cone, the resistance decreases. Sufficient confidence has now been obtained in the accuracy and precision of the results and the effect of other parameters on the results should be examined.

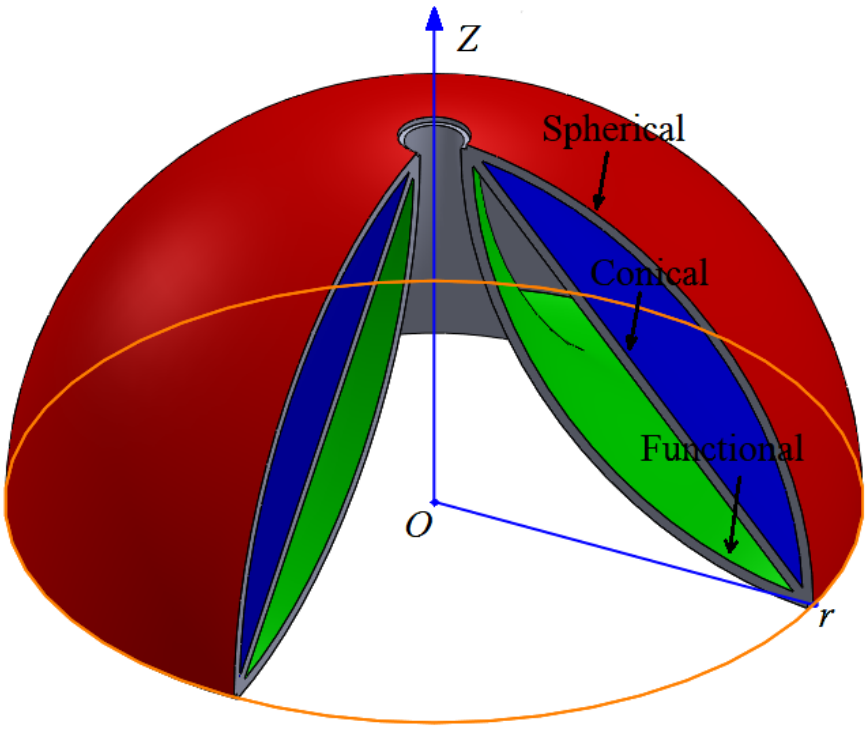

Fig. 15. Schematic view of spherical, conical and functional shell structures

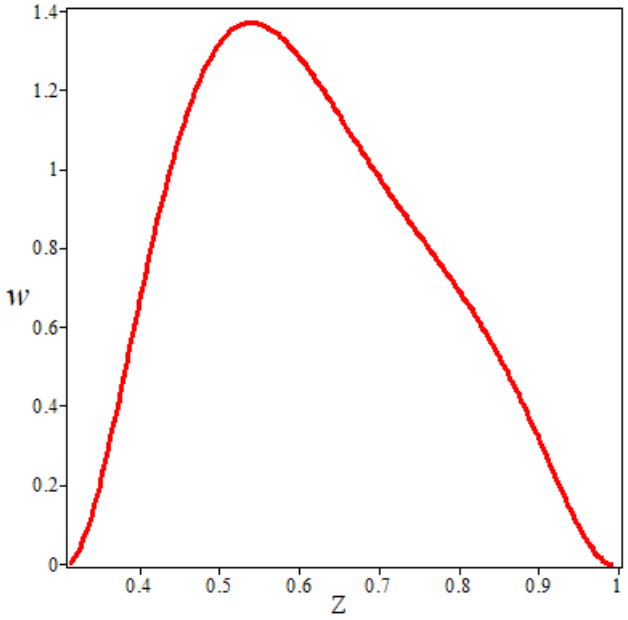

Fig. 16. Deflection of spherical shell structures

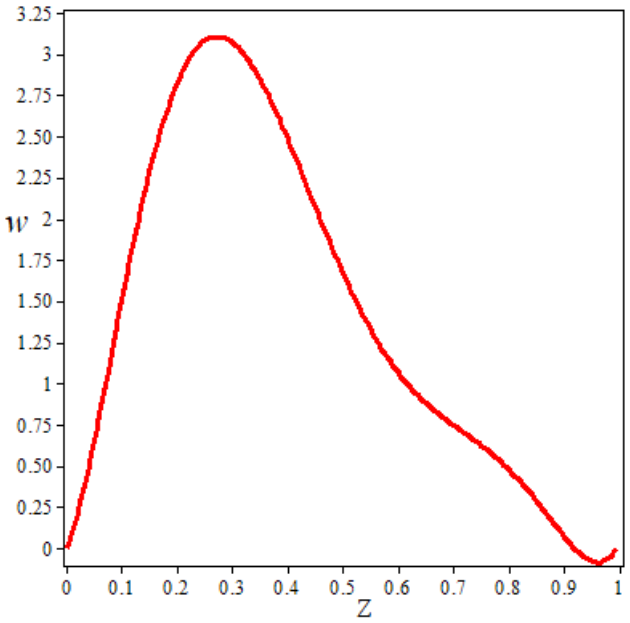

Fig. 17. Deflection of conical shell structures

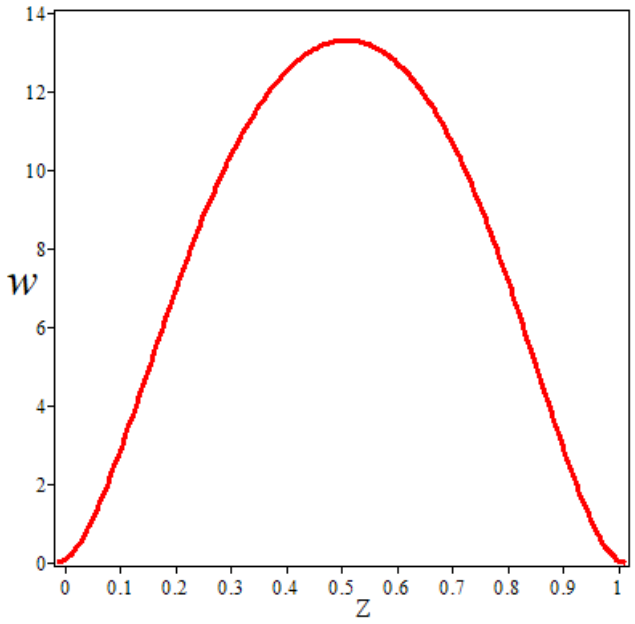

Fig. 18. Deflection of functional shell structures

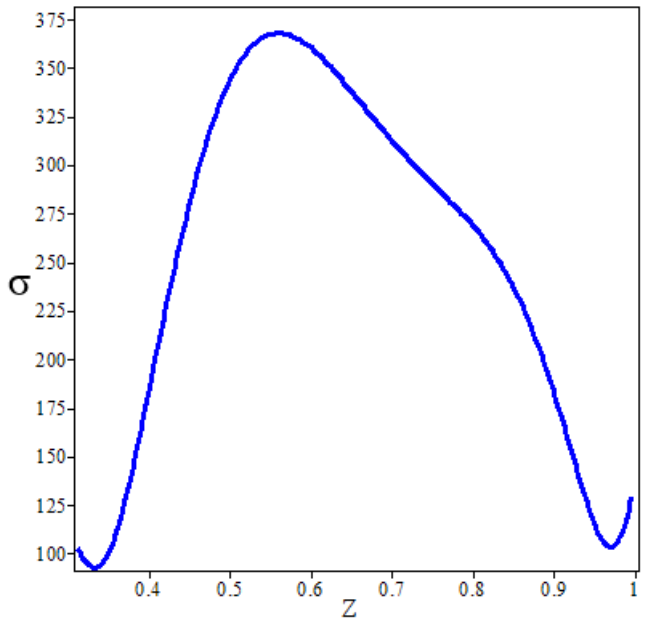

Fig. 19. von Mises stress of spherical shell structures

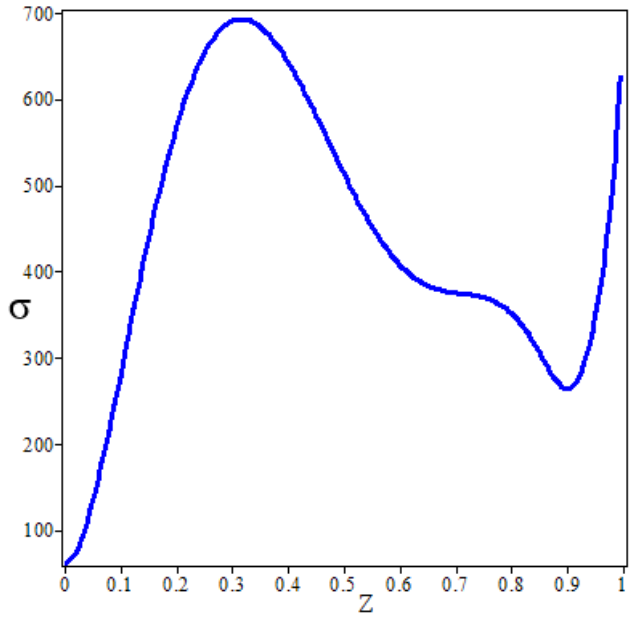

Fig. 20. von Mises stress of conical shell structures

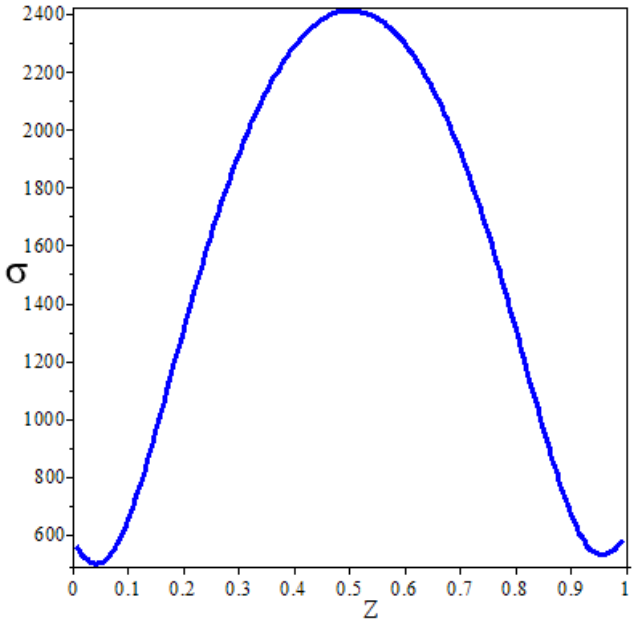

Fig. 21. von Mises stress of functional shell structures

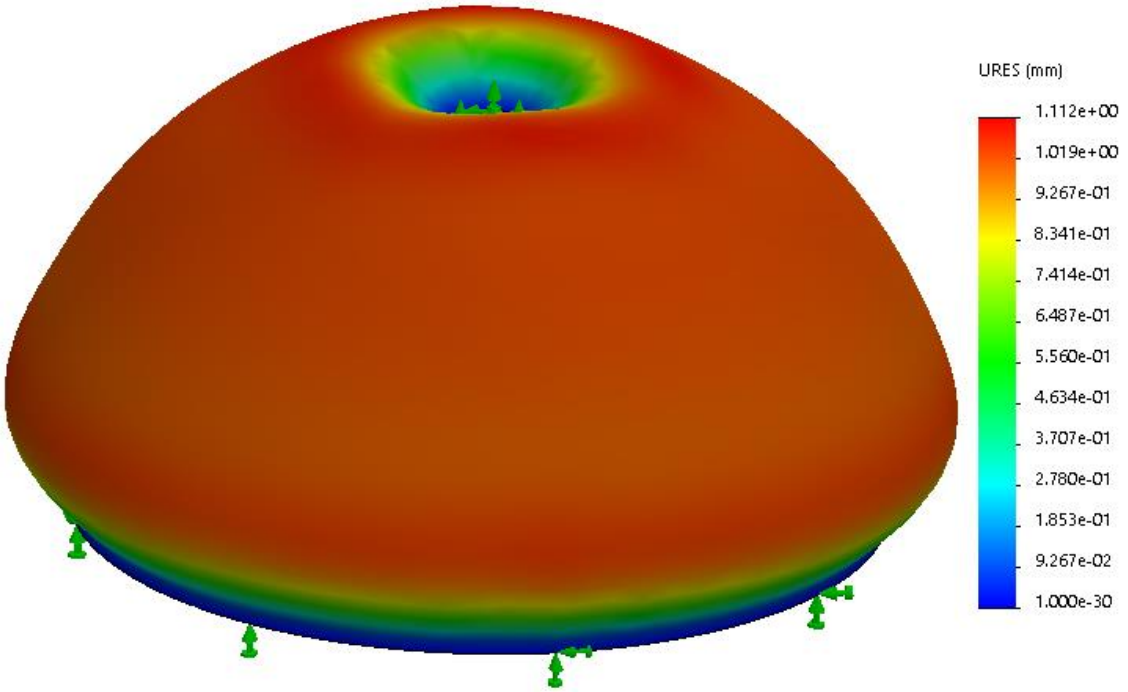

Fig. 22. Deflection FEM results of spherical shell structures

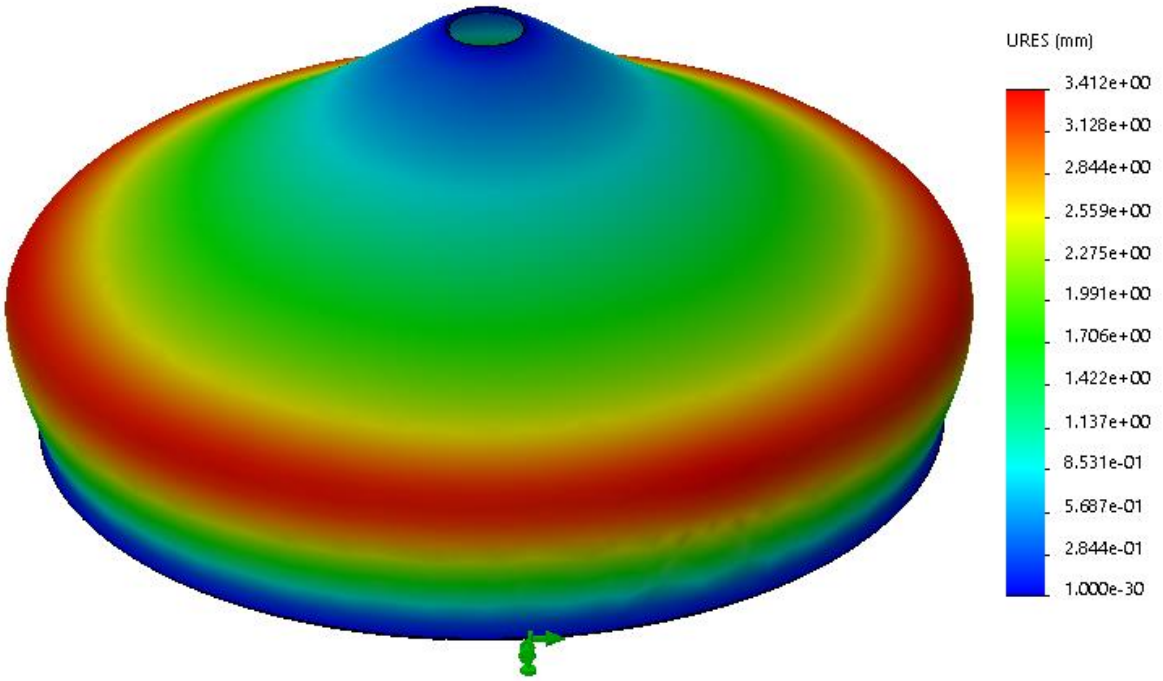

Fig. 23. Deflection FEM results of conical shell structures

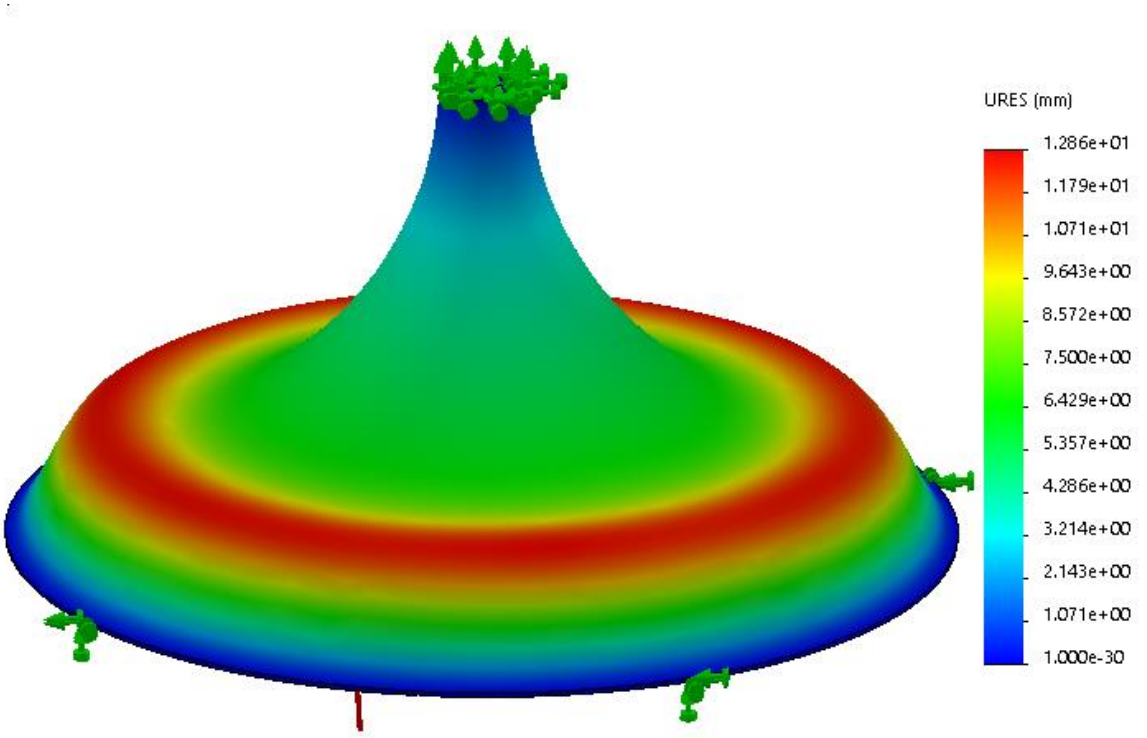

Fig. 24. Deflection FEM results of functional shell structures

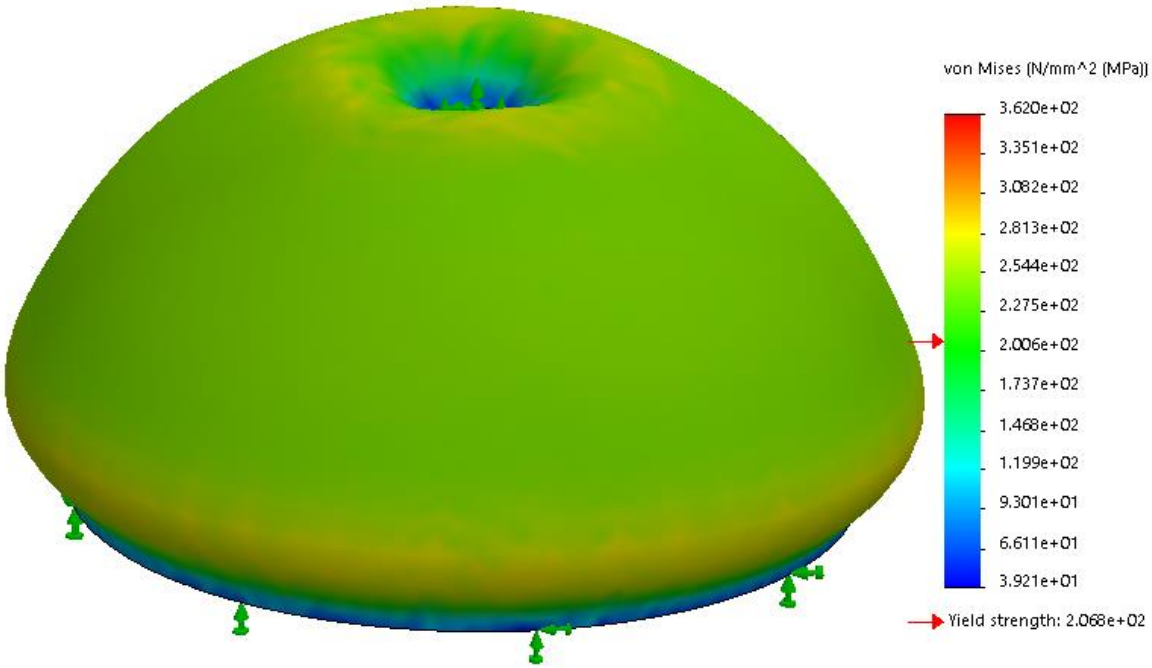

Fig. 25. von Mises FEM stress results of spherical shell structures

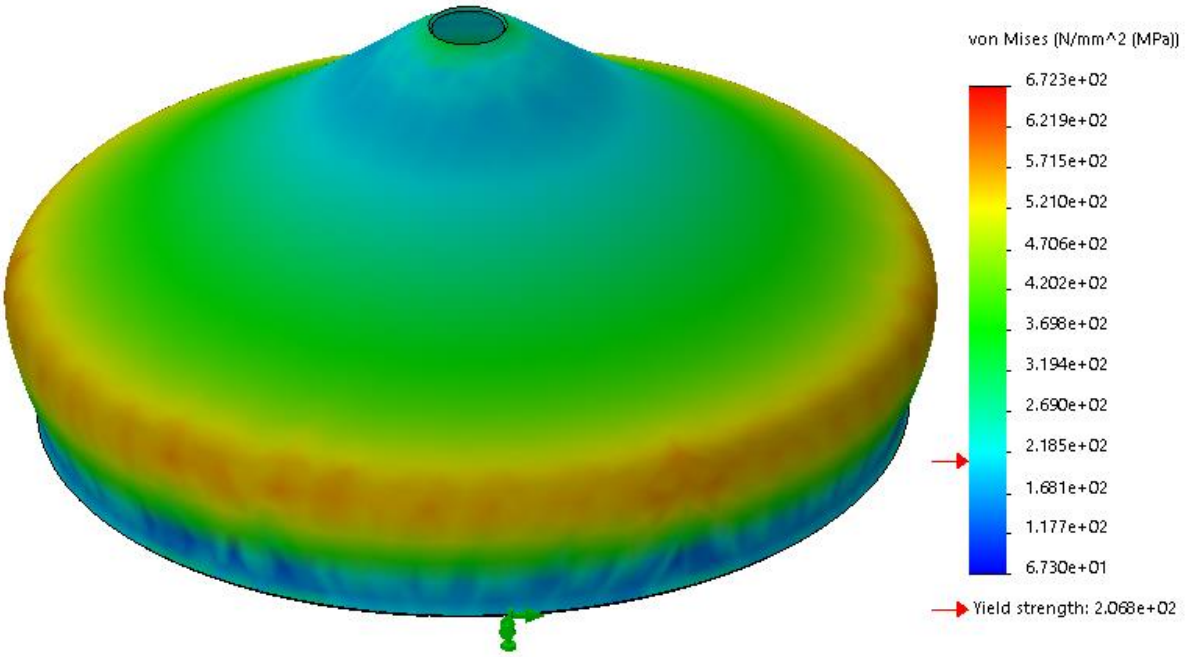

Fig. 26. von Mises FEM stress results of conical shell structures

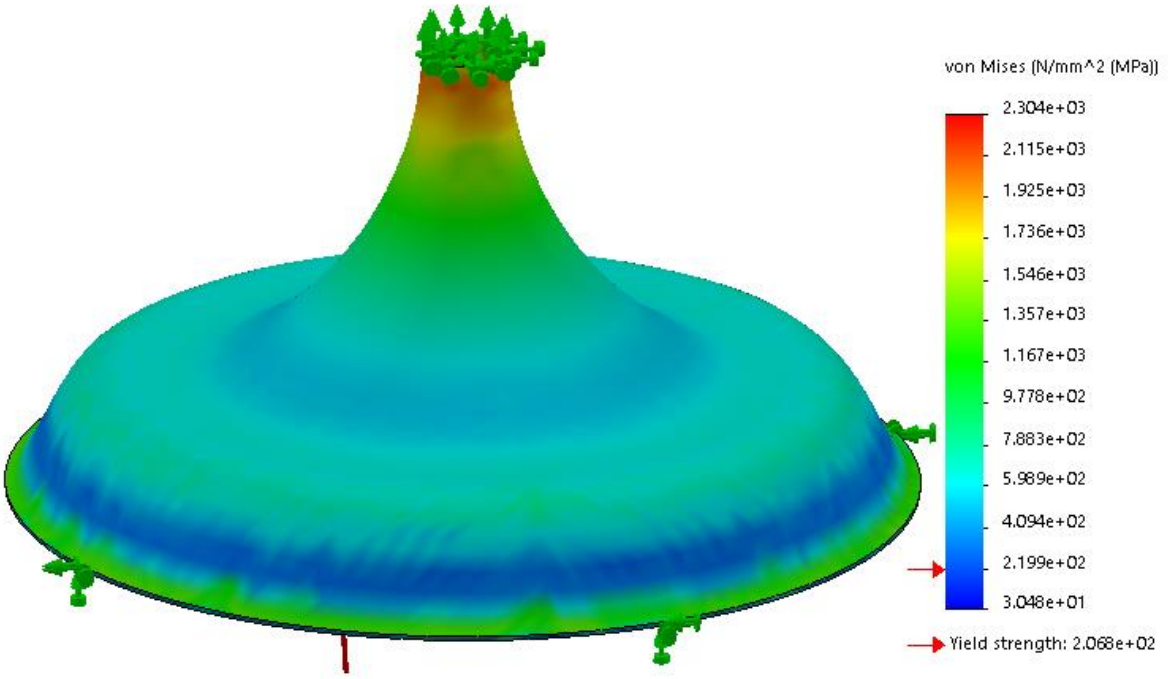

Fig. 27. von Mises FEM stress results of functional shell structures

5.4. Investigation of effective parameters

As mentioned earlier, the basic equations introduced in this study are generalized and are extracted in a dynamic state. One of the important and influential factors in the dynamic analysis of a shell structure is the effect of the rotational speed of the structure on its strength and also the deformations that occur in it. Other factors affecting the results will be discussed in the following numerical results. For the three structures discussed above, if they rotate around the central axis of the rotation, it is expected to be increased the deformations created in them and decreased the strength of the structure.

Figs. 28 and 29 show the dimensionless deflections, as well as the dimensionless von Mises stresses in the structure relative to the changes in rotational velocity. Hereafter, the structure's geometrical and material specifications are the same as the previous analysis in Figs. 16–21. In fact, w_ω represents the amount of deflection created in a rotating structure with a rotational velocity n relative to the state in which the structure is considered stationary and without rotation. The same is true for von Mises dimensionless stresses. It is observed that with increasing rotational speed n, the values of w_ω and σ_ω increase with an accelerating slope and ascending. The changes are nonlinear, in other words, the higher the rotational speed, the greater the effect on productivity and dimensionless stress.

$$w_\omega = \frac{w_{n\neq 0}}{w_{n=0}}; \sigma_\omega = \frac{\sigma_{n\neq 0}}{\sigma_{n=0}} \tag{29}$$

In the case of the three spherical, cone, and functional cone structures, the effect of the rotational speed on the results in the spherical structure will be greater than the rest of the structures. At the beginning of the changes, it is observed that the results for all three structures will be almost the same with a good approximation. But as the speed of the rotation increases, the results diverge. It is noteworthy that the results for rotational velocity changes for both spherical and functional cone structures are almost identical and will differ slightly. However, at a rotation speed of about $3000\ rpm$, it is observed that the dimensionless deflection for the

spherical structure is about 2.6, which is about 2.1 for the conical and functional conical structures. The difference between the two results shows a reduction of about twenty percent. Another important point is that the results for Figs. 28 and 29 show almost the same behavior. In other words, the effect of rotational speed will be the same for dimensionless deflection results and dimensionless stresses. In general, according to the above, it can be concluded that the rotational speed of a structure has a significant effect on increasing the deformation of the structure as well as reducing its strength, which must be considered to prevent it.

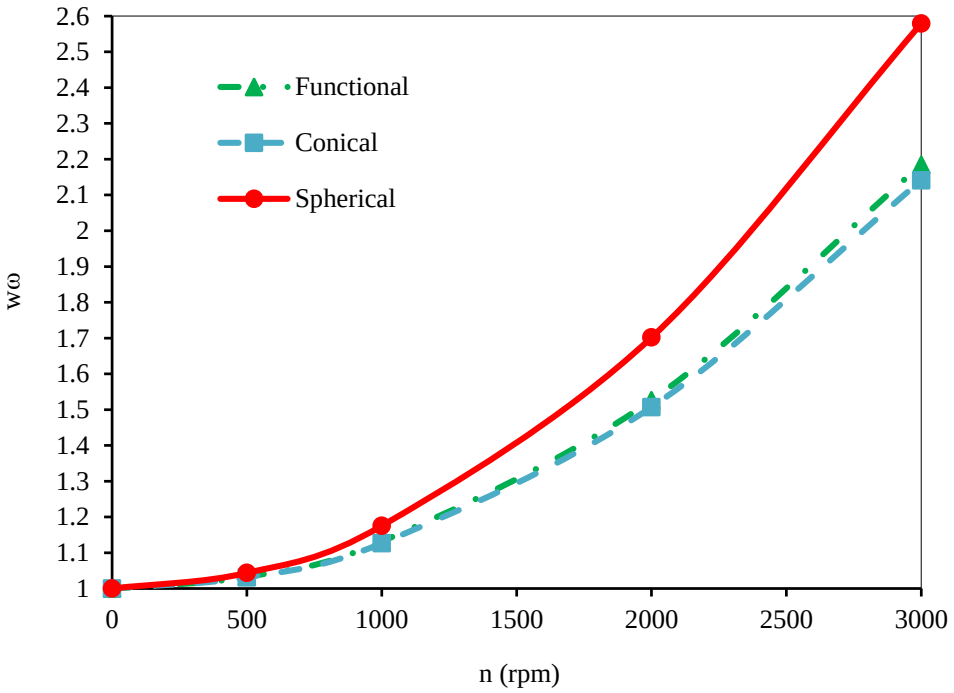

Fig. 28. Dimensionless deflection results (w_ω) versus the angular rotation speed (n) for spherical, conical and functional shell structures

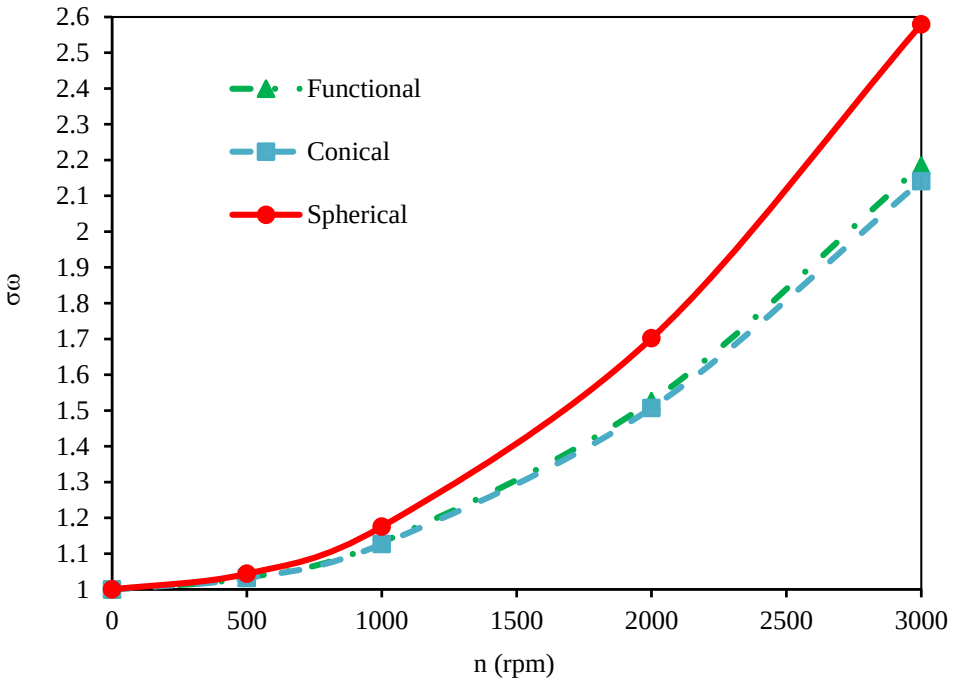

Fig. 29. Dimensionless von Mises results (σ_ω) versus the angular rotation speed (n) for spherical, conical and functional shell structures

In order to increase the accuracy of the results, especially in the case of large deformations, nonlinear analysis has been used in this study. Although the use of nonlinear analysis increases the accuracy of the results, in a situation where the results of nonlinear and linear analysis will not be much different and given that the speed of calculations in nonlinear analysis will be much higher than linear analysis, Linear results can be used with high accuracy.

In the previous section, the effect of the rotational speed of the structure on the results of deformation and stress of von Mises was investigated. Now, considering the conditions of the previous problem, the results of both linear and nonlinear analyzes for deformations can be seen in Fig. 30. The dimensionless parameter R_s represents the ratio of the results of the deformation in the nonlinear analytical mode to the linear analysis ($R_s = \frac{w_{nonlinear}}{w_{linear}}$). As can be expected, the results of the nonlinear analysis should be less than the results of linear analysis. Therefore, the

change interval of R_s will be $0 < R_s < 1$. According to Fig. 30, it can be seen that the changes of R_s for the functional cone structure will be more severe than the other two structures. Comparing the two spherical and conical structures, as can be seen, nonlinear analysis is more important for the spherical structure with a small difference (by increasing the rotational speed of the structure). In the case of the functional cone structure, at the beginning of the rotational velocity changes, the slope of the changes is gentle and descending, and from the rotational velocity $n = 1000\ rpm$ onwards, the slope of the changes suddenly experiences a sharp drop. The difference between the results of linear and nonlinear analysis at the rotational speed $n = 3000\ rpm$ for the structure of a functional cone is about ten percent. This value is significant and if the linear analysis is used, there will be a lot of error in the results and there is no choice but to use nonlinear analysis. Even at zero rotational velocities, and when the structure is static and loaded statically, about 3.5% of the difference between the results of linear and nonlinear analyzes is observed in the case of a functional cone structure. Of course, according to Fig. 30, the remarkable result is that in the case of two spherical and conical structures, according to the loading conditions of the problem, the results of the two linear and nonlinear analyzes are not much different (a topic mentioned earlier) and due to simplicity in the linear analysis, the results of linear analysis can be used, the results to which can be obtained faster. The results obtained in this section can be expected in advance because, as mentioned earlier and concluded, the deformation of the functional cone structure is much greater than the other two structures (spherical and conical) under the same loading conditions and due to large deformations created in it, the results of two linear and nonlinear analyzes for functional cone must be more distant from each other than the other two structures, which is the same conclusion in this section according to Fig. 30.

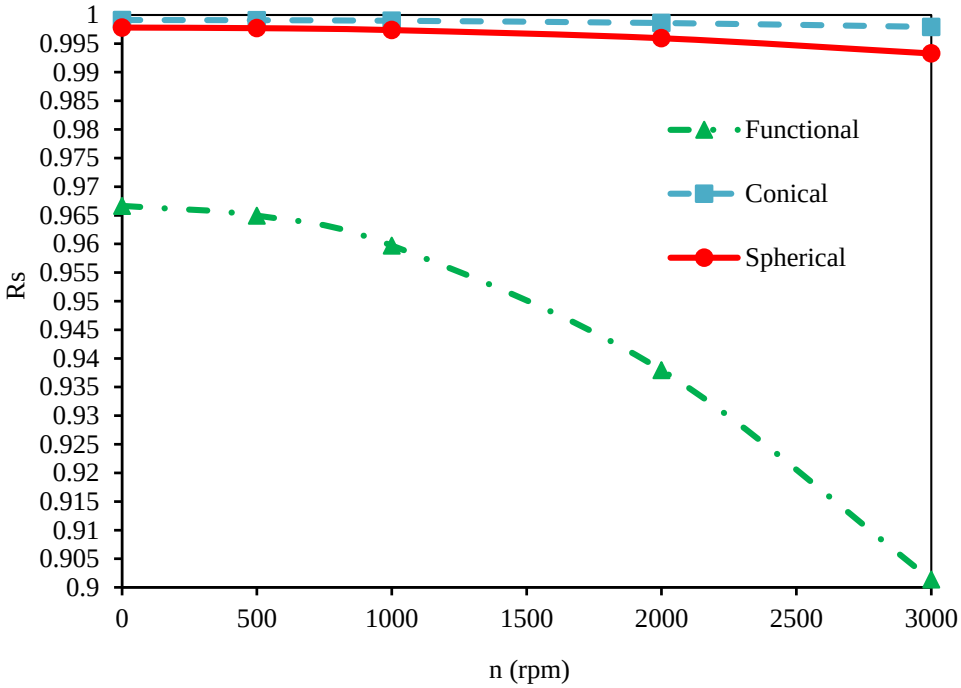

Fig. 30. Nonlinear to linear results of deflection (R_s) versus the angular rotation speed (n) for spherical, conical and functional shell structures

Environmental factors such as ambient temperature have a significant effect on determining the mechanical strength of a structure, which is expected to decrease with increasing ambient temperature due to increased deformation of the structure from its resistance to mechanical loads. Of course, this issue should be carefully considered in the form of different structures. Figs. 31, 32 for this purpose show the dimensional changes and dimensionless von Mises stress for the three spherical, conical and functional cone structures in exchange for increasing the temperature difference. It is observed that with increasing the temperature difference of the system, the results of dimensionless deflection and stress increase. Here, dimensionless deflections and stresses indicate those in the case where there is a temperature difference in the structure compared to the case where the temperature difference is zero. It is observed that the changes in both Figs. 31, 32 are linear, although in the case of the functional cone structure between the two temperatures $100 < \Delta T < 200\,°C$ there is a slight deviation

from the linear state, the slope of the changes will be similar to $\Delta T < 100\ ^{\circ}C$ (A slight increase in slope is observed). By comparing the results of the three structures in question, it is observed that the ambient temperature has the greatest effect on the spherical structure and has the least effect on the functional cone structure. Therefore, in spherical structures, the effects of temperature changes should be considered more. For example, at a temperature difference of $400\ ^{\circ}C$, the temperature of the environment affects deformations created in the spherical structure about 7 times compared to $\Delta T = 0$, which is about 5 times in the case of the conical structure and in relation to the functional conical structure, it is about 3.5 percent increase in deformation rate. Dimensional von Mises stress changes relative to dimensionless deflections (Fig. 32 versus Fig. 31) show a reduction of approximately 50%. In other words, increasing the ambient temperature causes the structure to deform, which at the same time increases the stress in the structure. But the increase in deformation will be about twice as much as the increase in thermal stresses created in the structure.

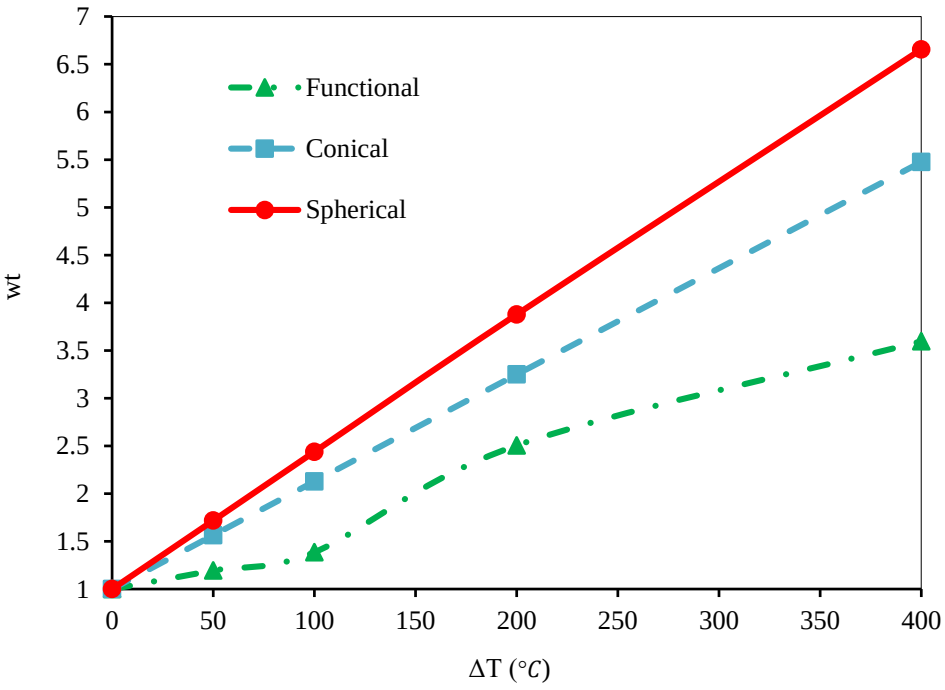

Fig. 31. Nondimensional thermal deflection (w_t) versus the temperature differences (ΔT) for spherical, conical and functional shell structures

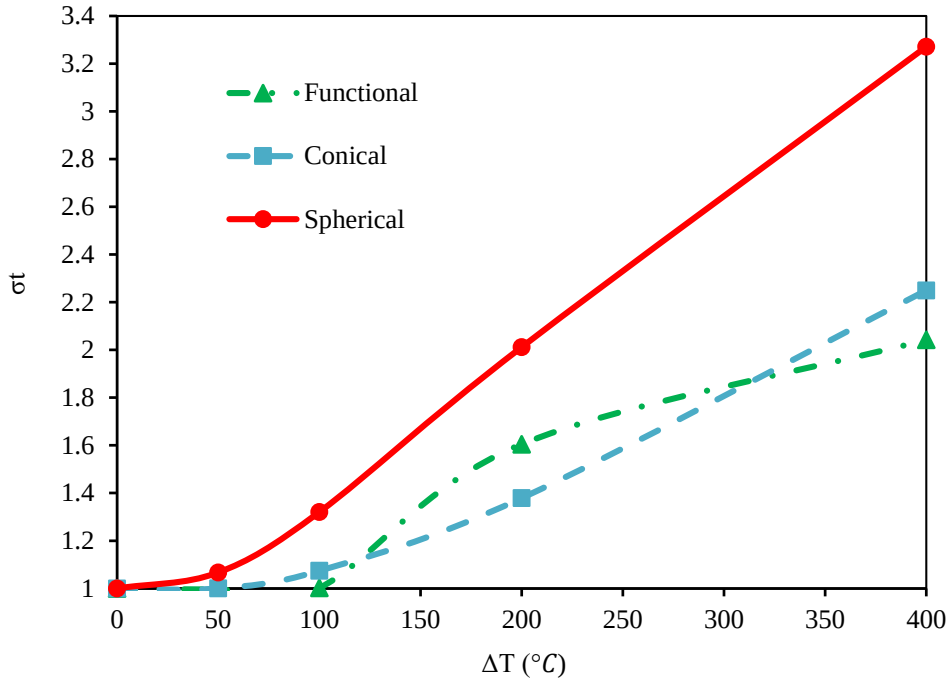

Fig. 32. Nondimensional thermal stress (σ_t) versus the temperature differences (ΔT) for spherical, conical and functional shell structures

In this study, the effects related to the functional grading property of the composite material (FGM) have also been considered. The functional grading of the material from ceramic to metal within the thickness of the structure is considered. The metal and ceramic amounts of the Young's elasticity modulus are assumed as $E_M = 190\ GPa$ and $E_c = 0.85\ GPa$ and the Poisson's ratio for both of the ceramic and metal properties are the same as $\nu_c = \nu_M = 0.29$. Figs. 33, 34 show the dimensionless deflections and stresses of von Mises with respect to the increase of the ζ parameter, which indicates the intensity of the changes from the ceramic to the metal state in the FGM material. Figs. 33, 34 show the mentioned effects for different values of temperature changes, which are observed (according to Fig. 33) by increasing the ζ-parameter,

first the dimensionless deflection w_ζ increases with a steep slope and from the value of $\zeta = 10$ onwards, the changes of w_ζ will be accompanied by a gentle slope and the intensity of the changes will decrease and practically increasing the value of ζ will no longer affect the increase of w_ζ.

$$w_\zeta = \frac{w_{\zeta \neq 0}}{w_{\zeta = 0}}; \sigma_\zeta = \frac{\sigma_{\zeta \neq 0}}{\sigma_{\zeta = 0}} \tag{30}$$

The behavior of the structure (here considered as spherical structure) shows almost a trend of change in exchange for different temperature differences. However, it is observed that as the temperature difference increases, the dimensionless deflections value of w_ζ will decrease. Of course, the decrease in w_ζ in exchange for the increase in ΔT is not linear and is accompanied by a decrease (because the decrease in w_ζ from $\Delta T = 0$ to $\Delta T = 100\ ^\circ C$ is approximately equal to the decrease in w_ζ from $\Delta T = 100\ ^\circ C$ to $\Delta T = 300\ ^\circ C$). In other words, with increasing the same values of the ΔT, the rate of decrease of the w_ζ parameter is not the same. The contents of the diagrams in Fig. 34 are exactly the opposite of Fig. 33. In other words, the value ζ for dimensionless von Mises stress σ_ζ (the ratio of von Mises stress for $\zeta \neq 0$ to the stress for the value $\zeta = 0$) will decrease and the decreasing value of σ_ζ for a larger temperature difference (here $\Delta T = 300\ ^\circ C$) will be more severe. It is important to note that the dimensionless stress σ_ζ is almost equal to a unit with a very small difference of ζ for two values of temperature difference $\Delta T = 0$ and $\Delta T = 100\ ^\circ C$. In other words, it can be said that the von Mises stress in these two cases for different values of the parameter ζ is equal to the von Mises stress of the structure in the case that $\zeta = 0$. It can be said that the stresses created in the FGM structure for the low-temperature difference are independent of the value of ζ and the only difference between the results is obtained when the structure is exposed to an environment with high-

temperature differences, in which case the thermal stresses created in the structure will be impressive.

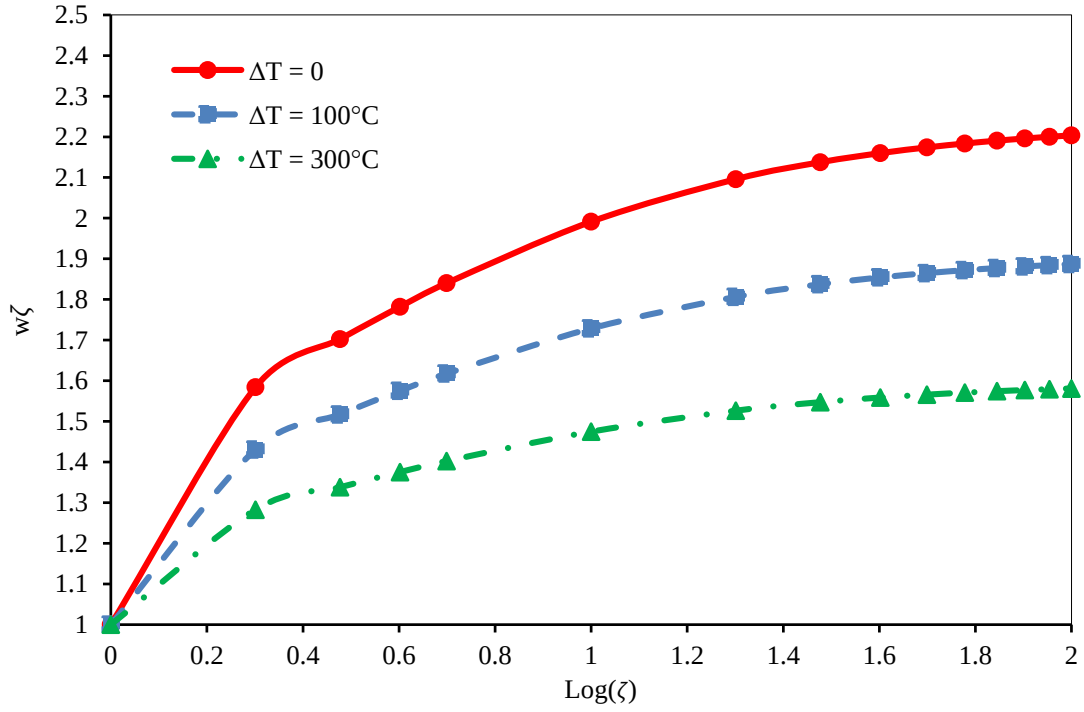

Fig. 33. Nondimensional deflection (w_ζ) versus the increase of ζ parameter in FG material for different temperature differences (ΔT)

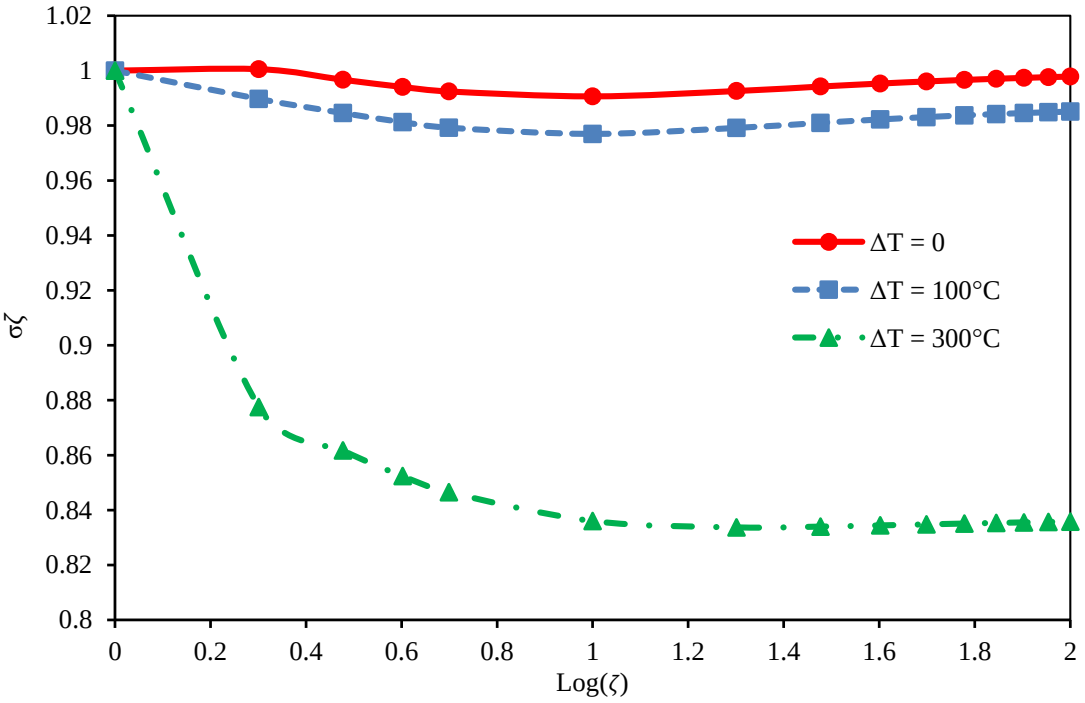

Fig. 34. Nondimensional von Mises stress (σ_ζ) versus the increase of ζ parameter in FG material for different temperature differences (ΔT)

In general, countless structures can be studied using the basic equations mentioned in this study and also the effect of factors affecting the problem that can be very diverse. The main advantage of the basic equations presented in the current study is the ability to analyze any type of shell structure with different geometries, which neutralizes the researchers' use of coordinate systems and the relevant formulation of each coordinate system, and any type of analysis can be entered in this research and obtained the specific results of those conditions.

6. Conclusions and remarks

In this research, a general solution and comprehensive formulation for mechanical dynamic analysis of different types of shell structures with any desired geometry are presented. Therefore, it is no longer necessary to use the system of different coordinates related to different types of geometry, and with a formula system that is partial differential equations, any shell

structure can be examined mechanically. The cross-section of the shell structure is considered as an arbitrary function with any relation as $z = f(r)$. This arbitrary function rotates around the z-axis (the angle of rotation is considered from zero to 2π) and a shell structure forms. The governing equations are obtained using the principle of minimum potential energy and are solved by the efficient SAPM method. The most important parts of this research are the following:

- Analysis of any shell structure with a variety of geometric shapes.
- Analysis of the elliptical structure using the equations presented in this study, which previously the analysis of this type of structures has been associated with many challenges.
- Nonlinear analysis has the most impact on the functional shell structure between three spherical, conical, and functional structures.
- Thermal analysis of various shell-shaped structures has been investigated and it is concluded that spherical structure will be affected more by thermal loads.
- The dynamic effects on the analysis are considered and the dynamic loads created by the rotation of the structure are investigated.

Acknowledgements

V.A.E acknowledges the support of the Government of the Russian Federation (contract No. 14.Z50.31.0046).

Data availability

The raw/processed data required to reproduce these findings cannot be shared at this time as the data also forms part of an ongoing study.

References

[1] M. Malikan, V. A. Eremeyev, A new hyperbolic-polynomial higher-order elasticity theory for mechanics of thick FGM beams with imperfection in the material composition, Composite Structures, 249 (2020) 112486.

[2] Sh. Dastjerdi, M. Malikan, R. Dimitri, F. Tornabene, Nonlocal elasticity analysis of moderately thick porous functionally graded plates in a hygro-thermal environment, Composite Structures, 255 (2021) 112925.

[3] Sh. Dastjerdi, B. Akgöz, New static and dynamic analyses of macro and nano FGM plates using exact three-dimensional elasticity in thermal environment, Composite Structures, 192 (2018) 626–641.

[4] M. Malikan, R. Dimitri, F. Tornabene, Nonlocal three-dimensional theory of elasticity for buckling behavior of functionally graded porous nanoplates using volume integrals, Materials Research Express, 5 (2018) 095006.

[5] Sh. Dastjerdi, Y. Tadi Beni, M. Malikan, A comprehensive study on nonlinear hygro-thermo-mechanical analysis of thick functionally graded porous rotating disk based on two quasi-three-dimensional theories, Mechanics Based Design of Structures and Machines, An International Journal, https://doi.org/10.1080/15397734.2020.1814812.

[6] M. Yamanouchi, M. Koizumi, T. Hirai, I. Shiota, Proceedings of the First International Symposium on Functionally Gradient Materials, FGM, 1990, Japan, Organized and Sponsored by Functionally Gradient Materials Forum.

[7] M. Koizumi, FGM activities in Japan, Composites Part B: Engineering, 28 (1997) 1–4.

[8] W. A. Kaysser, B. Ilschner, FGM Research Activities in Europe, MRS Bull, 20 (1995) 22–26.

[9] M. Koizumi, M. Niino, Overview of FGM Research in Japan, MRS Bull, 20 (1995) 19–21.

[10] Y. Miyamoto, W.A. Kaysser, B.H. Rabin, A. Kawasaki, R.G. Ford Functionally Graded Materials: Design, Processing and Applications, Springer, Springer Science & Business Media, 5 (2013) 1–317.

[11] H. S. Shen, Postbuckling analysis of axially-loaded functionally graded cylindrical shells in thermal environments, Composites Science and Technology, 62 (2002) 977–987.

[12] H. S. Shen, Postbuckling analysis of pressure-loaded functionally graded cylindrical shells in thermal environments, Engineering Structures, 25 (2003) 487–497.

[13] M. Amabili, A comparison of shell theories for large-amplitude vibrations of circular cylindrical shells: Lagrangian approach, Journal of Sound and Vibration, 264 (2003) 1091‑1125.

[14] R. A. Arciniega, J. N. Reddy, Large deformation analysis of functionally graded shells, International Journal of Solids and Structures, 44 (2007) 2036–2052.

[15] M. M. Najafizadeh, M. R. Isvandzibaei, Vibration of functionally graded cylindrical shells based on higher order shear deformation plate theory with ring support, Acta Mechanica, 191 (2007) 75–91.

[16] M. Darabi, M. Darvizeh, A. Darvizeh, Non-linear analysis of dynamic stability for functionally graded cylindrical shells under periodic axial loading, Composite Structures, 83 (2008) 201–211.

[17] H. S. Shen, Torsional buckling and postbuckling of FGM cylindrical shells in thermal environments, International Journal of Non-Linear Mechanics, 44 (2009) 644 – 657.

[18] H. Matsunaga, Free vibration and stability of functionally graded circular cylindrical shells according to a 2D higher-order deformation theory, Composite Structures, 88 (2009) 519–531.

[19] Ye. Kurylov, M. Amabili, Polynomial versus trigonometric expansions for nonlinear vibrations of circular cylindrical shells with different boundary conditions, Journal of Sound and Vibration, 329 (2010) 1435–1449.

[20] S. M. R. Khalili, A. Davar, K. Malekzadeh Fard, Free vibration analysis of homogeneous isotropic circular cylindrical shells based on a new three-dimensional refined higher-order theory, International Journal of Mechanical Sciences, 56 (2012) 1–25.

[21] G. Jin, X. Xie, Zh. Liu, The Haar wavelet method for free vibration analysis of functionally graded cylindrical shells based on the shear deformation theory, Composite Structures, 108 (2014) 435–448.

[22] K. Mohammadi, M. Mahinzare, K. Ghorbani, M. Ghadiri, Cylindrical functionally graded shell model based on the first order shear deformation nonlocal strain gradient elasticity theory, Microsystem Technologies, 24 (2018) 1133–1146.

[23] W. Chen, D. Liu, S. Kitipornchai, J. Yang, Bifurcation of pressurized functionally graded elastomeric hollow cylinders, Composites Part B: Engineering, 109 (2017) 259–276.

[24] A. H. Sofiyev, On the solution of the dynamic stability of heterogeneous orthotropic visco-elastic cylindrical shells, Composite Structures, 206 (2018) 124–130.

[25] E. Hasrati, R. Ansari, J. Torabi, A novel numerical solution strategy for solving nonlinear free and forced vibration problems of cylindrical shells, Applied Mathematical Modelling, 53 (2018) 653–672.

[26] M. Khorsand, K. Fu, Y. Tang, Multi-directional functionally graded materials for enhancing the durability of shell structures, International Journal of Pressure Vessels and Piping, 175 (2019) 103926.

[27] R. Ansari, J. Torabi, Semi-analytical postbuckling analysis of polymer nanocomposite cylindrical shells reinforced with functionally graded graphene platelets, Thin-Walled Structures, 144 (2019) 106248.

[28] M. Malikan, M. Krasheninnikov, V. A. Eremeyev, Torsional stability capacity of a nano-composite shell based on a nonlocal strain gradient shell model under a three-dimensional magnetic field, International Journal of Engineering Science, 148 (2020) 103210.

[29] B. Karami, M. Janghorban, On the mechanics of functionally graded nanoshells, International Journal of Engineering Science, 153 (2020) 103309.

[30] A. Mohamadi, M. Shahgholi, F. Ashenai Ghasemi, Nonlinear vibration of axially moving simply-supported circular cylindrical shell, Thin-Walled Structures, 156 (2020) 107026.

[31] L. Xuebin, A new approach for free vibration analysis of thin circular cylindrical shell, Journal of Sound and Vibration, 296 (2006) 91–98.

[32] F. Pellicano, Dynamic stability and sensitivity to geometric imperfections of strongly compressed circular cylindrical shells under dynamic axial loads, Communications in Nonlinear Science and Numerical Simulation, 14 (2009) 3449–3462.

[33] F. Tornabene, E. Viola, D. J. Inman, 2-D differential quadrature solution for vibration analysis of functionally graded conical, cylindrical shell and annular plate structures, Journal of Sound and Vibration, 328 (2009) 259–290.

[34] W. Zhang, Y. X. Hao, J. Yang, Nonlinear dynamics of FGM circular cylindrical shell with clamped–clamped edges, Composite Structures, 94 (2012) 1075–1086.

[35] G. G. Sheng, X. Wang, An analytical study of the non-linear vibrations of functionally graded cylindrical shells subjected to thermal and axial loads, Composite Structures, 97 (2013) 261–268.

[36] A. H. Sofiyev, Nonlinear free vibration of shear deformable orthotropic functionally graded cylindrical shells, Composite Structures, 142 (2016) 35–44.

[37] K. Xie, M. Chen, L. Zhang, D. Xie, Free and forced vibration analysis of non-uniformly supported cylindrical shells through wave based method, International Journal of Mechanical Sciences, 128–129 (2017) 512–526.

[38] Y. Wang, D. Wu, Free vibration of functionally graded porous cylindrical shell using a sinusoidal shear deformation theory, Aerospace Science and Technology, 66 (2017) 83–91.

[39] G. G. Sheng, X. Wang, Nonlinear response of fluid-conveying functionally graded cylindrical shells subjected to mechanical and thermal loading conditions, Composite Structures, 168 (2017) 675–684.

[40] S. Sahmani, M. Mohammadi Aghdam, Imperfection sensitivity of the size-dependent postbuckling response of pressurized FGM nanoshells in thermal environments, Archives of Civil and Mechanical Engineering, 17 (2017) 623–638.

[41] S. Sahmani, M. M. Aghdam, Nonlocal strain gradient shell model for axial buckling and postbuckling analysis of magneto-electro-elastic composite nanoshells, Composites Part B: Engineering, 132 (2018) 258–274.

[42] J. Zhao, K. Choe, Y. Zhang, A. Wang, Ch. Lin, Q. Wang, A closed form solution for free vibration of orthotropic circular cylindrical shells with general boundary conditions, Composites Part B: Engineering, 159 (2019) 447–460.

[43] A. H. Sofiyev, D. Hui, On the vibration and stability of FGM cylindrical shells under external pressures with mixed boundary conditions by using FOSDT, Thin-Walled Structures, 134 (2019) 419–427.

[44] R. Salahifar, M. Mohareb, Generalized theory for the dynamic analysis of thin shells with application to circular cylindrical geometries, Thin-Walled Structures, 139 (2019) 347–361.

[45] W. Ye, J. Liu, Q. Zang, G. Lin, Magneto-electro-elastic semi-analytical models for free vibration and transient dynamic responses of composite cylindrical shell structures, Mechanics of Materials, 148 (2020) 103495.

[46] G. Z. Voyiadjis, P. Woelke, A refined theory for thick spherical shells, International Journal of Solids and Structures, 41 (2004) 3747–3769.

[47] D. H. Bich, H. V. Tung, Non-linear axisymmetric response of functionally graded shallow spherical shells under uniform external pressure including temperature effects, International Journal of Non-Linear Mechanics, 46 (2011) 1195–1204.

[48] D. H. Bich, D. V. Dung, L. K. Hoa, Nonlinear static and dynamic buckling analysis of functionally graded shallow spherical shells including temperature effects, Composite Structures, 94 (2012) 2952–2960.

[49] R. Zaera, J. Fernández-Sáez, J. A. Loya, Axisymmetric free vibration of closed thin spherical nano-shell, Composite Structures, 104 (2013) 154–161.

[50] Ö. Civalek, Geometrically nonlinear dynamic and static analysis of shallow spherical shell resting on two-parameters elastic foundations, International Journal of Pressure Vessels and Piping, 113 (2014) 1–9.

[51] N. Fantuzzi, S. Brischetto, F. Tornabene, E. Viola, 2D and 3D shell models for the free vibration investigation of functionally graded cylindrical and spherical panels, Composite Structures, 154 (2016) 573–590.

[52] E. Ghavanloo, H. Rafii-Tabar, S. Ahmad Fazelzadeh, New insights on nonlocal spherical shell model and its application to free vibration of spherical fullerene molecules, International Journal of Mechanical Sciences, 161–162 (2019) 105046.

[53] B. M. Shinde, A. S. Sayyad, Static Deformation of Orthotropic Spherical Shell Using Fifth Order Shear and Normal Deformation Theory, Materials Today: Proceedings 21 (2020) 1123–1127.

[54] Sh. Dastjerdi, B. Akgöz, Ö. Civalek, On the shell model for human eye in Glaucoma disease, International Journal of Engineering Science, 158 (2021) 103414.

[55] L. Qi, Sh. Zhou, A size-dependent spherical microshell model based on strain gradient elasticity theory, European Journal of Mechanics - A/Solids, 84 (2020) 104087.

[56] R. Shahsiah, M. R. Eslami, M. Sabzikar Boroujerdy, Thermal instability of functionally graded deep spherical shell, Archive of Applied Mechanics, 81 (2011) 1455–1471.

[57] P. Malekzadeh, Y. Heydarpour, Free vibration analysis of rotating functionally graded truncated conical shells, Composite Structures, 97 (2013) 176–188.

[58] S. Kamarian, M. Salim, R. Dimitri, F. Tornabene, Free vibration analysis of conical shells reinforced with agglomerated Carbon Nanotubes, International Journal of Mechanical Sciences, 108–109 (2016) 157–165.

[59] Q. Dai, Q. Cao, Y. Chen, Frequency analysis of rotating truncated conical shells using the Haar wavelet method, Applied Mathematical Modelling, 57 (2018) 603–613.

[60] R. Ansari, J. Torabi, E. Hasrati, Postbuckling analysis of axially-loaded functionally graded GPL-reinforced composite conical shells, Thin-Walled Structures, 148 (2020) 106594.

[61] A. H. Sofiyev, On the vibration and stability behaviors of heterogeneous- CNTRC-truncated conical shells under axial load in the context of FSDT, Thin-Walled Structures, 151 (2020) 106747.

[62] T. Fu, X. Wu, Zh. Xiao, Zh. Chen, Dynamic instability analysis of porous FGM conical shells subjected to parametric excitation in thermal environment within FSDT, Thin-Walled Structures, 158 (2021) 107202.

[63] F. Tornabene, Free vibration analysis of functionally graded conical, cylindrical shell and annular plate structures with a four-parameter power-law distribution, Computer Methods in Applied Mechanics and Engineering, 198 (2009) 2911–2935.

[64] A. H. Sofiyev, N. Kuruoğlu, The stability of FGM truncated conical shells under combined axial and external mechanical loads in the framework of the shear deformation theory, Composites Part B: Engineering, 92 (2016) 463–476.

[65] M. Nejati, A. Asanjarani, R. Dimitri, F. Tornabene, Static and free vibration analysis of functionally graded conical shells reinforced by carbon nanotubes, International Journal of Mechanical Sciences, 130 (2017) 383–398.

[66] G. Watts, M. K. Singha, S. Pradyumna, Nonlinear bending and snap-through instability analyses of conical shell panels using element free Galerkin method, Thin-Walled Structures, 122 (2018) 452–462.

[67] A. H. Sofiyev, The buckling and vibration analysis of coating-FGM-substrate conical shells under hydrostatic pressure with mixed boundary conditions, Composite Structures, 209 (2019) 686–693.

[68] S. W. Yang, W. Zhang, Y.X. Hao, Y. Niu, Nonlinear vibrations of FGM truncated conical shell under aerodynamics and in-plane force along meridian near internal resonances, Thin-Walled Structures, 142 (2019) 369–391.

[69] Y. Yuan, K. Zhao, Y. Han, S. Sahmani, B. Safaei, Nonlinear oscillations of composite conical microshells with in-plane heterogeneity based upon a couple stress-based shell model, Thin-Walled Structures, 154 (2020) 106857.

[70] H. Zeighampour, Y. Tadi Beni, F. Mehralian, A shear deformable conical shell formulation in the framework of couple stress theory, Acta Mechanica, 226 (2015) 2607–2629.

[71] W. Jiang, D. Redekop, Static and vibration analysis of orthotropic toroidal shells of variable thickness by differential quadrature, Thin-Walled Structures, 41 (2003) 461–478.

[72] X. H. Wang, D. Redekop, Natural Frequencies Analysis of Moderately-Thick and Thick Toroidal Shells, Procedia Engineering, 14 (2011) 636–640.

[73] M. Shariyat, D. Asgari, Nonlinear thermal buckling and postbuckling analyses of imperfect variable thickness temperature-dependent bidirectional functionally graded cylindrical shells, International Journal of Pressure Vessels and Piping, 111–112 (2013) 310–320.

[74] F. Tornabene, N. Fantuzzi, M. Bacciocchi, R. Dimitri, Free vibrations of composite oval and elliptic cylinders by the generalized differential quadrature method, Thin-Walled Structures, 97 (2015) 114–129.

[75] D. H. Bich, D. G. Ninh, Post-buckling of sigmoid-functionally graded material toroidal shell segment surrounded by an elastic foundation under thermo-mechanical loads, Composite Structures, 138 (2016) 253–263.

[76] J. Torabi, R. Ansari, A higher-order isoparametric superelement for free vibration analysis of functionally graded shells of revolution, Thin-Walled Structures, 133 (2018) 169–179.

[77] Sh. Dastjerdi, B. Akgöz, Ö. Civalek, M. Malikan, V. A. Eremeyev, On the non-linear dynamics of torus-shaped and cylindrical shell structures, International Journal of Engineering Science, 156 (2020) 103371.

[78] P. M. Vuong, N. D. Duc, Nonlinear vibration of FGM moderately thick toroidal shell segment within the framework of Reddy's third order-shear deformation shell theory, International Journal of Mechanics and Materials in Design, 16 (2020) 245–264.

[79] H. Altenbach, V. A. Eremeyev, On the shell theory on the nanoscale with surface stresses, International Journal of Engineering Science, 49 (2011) 1294–1301.

[80] F. Tornabene, On the critical speed evaluation of arbitrarily oriented rotating doubly-curved shells made of functionally graded materials, Thin-Walled Structures, 140 (2019) 85–98.

[81] M. Caresta, N. J. Kessissoglou, Free vibrational characteristics of isotropic coupled cylindrical-conical shells, Journal of Sound and Vibration, 329 (2010) 733–751.

[82] Sh. Dastjerdi, B. Akgöz, Ö. Civalek, On the effect of viscoelasticity on behavior of gyroscopes, International Journal of Engineering Science, 149 (2020) 103236.

[83] V.N. Burlayenko, H. Altenbach, T. Sadowski, S.D. Dimitrova, Computational simulations of thermal shock cracking by the virtual crack closure technique in a functionally graded plate, Computational Materials Science, 116 (2016) 11–21.

[84] M. Bîrsan, H. Altenbach, T. Sadowski, V.A. Eremeyev, D. Pietras, Deformation analysis of functionally graded beams by the direct approach, Composites Part B: Engineering, 43 (2012) 1315–1328.

[85] V.N. Burlayenko, H. Altenbach, T. Sadowski, S.D. Dimitrova, A. Bhaskar, Modelling functionally graded materials in heat transfer and thermal stress analysis by means of graded finite elements, Applied Mathematical Modelling, 45 (2017) 422–438.

[86] V.N. Burlayenko, T. Sadowski, H. Altenbach, Efficient free vibration analysis of FGM sandwich flat panels with conventional shell elements, Mechanics of Advanced Materials and Structures (2021), https://doi.org/10.1080/15376494.2021.1909191.

[87] M.M. Aghdam, N. Shahmansouri, K. Bigdeli, Bending analysis of moderately thick functionally graded conical panels. Composite Structures 93 (2011) 1376–84.

[88] E. Viola, L. Rossetti, N. Fantuzzi, F. Tornabene, Static analysis of functionally graded conical shells and panels using the generalized unconstrained third order theory coupled with the stress recovery, Composite Structures, 112 (2014) 44–65.